Politecnico di Torino

POLITECNICO DI TORINO

Dipartimento di Ingegneria Meccanica e Aerospaziale

Laurea Magistrale in Ingegneria Meccanica

Modeling and Analysis of a Brake-by-Wire System in BEVs

SUPERVISOR
Prof. Giuseppe Quaglia
CO-SUPERVISOR
Ing. Bernardo Sessa (Teoresi)

CANDIDATE
Davide Galdi
S289598

Academic Year 2023-2024

This thesis was carried out in association with

Contents

List of Figures **iii**

List of Tables **vi**

1 Abstract **1**

2 Introduction **2**

2.1 Context 2

2.2 Scope of the thesis 4

2.3 Manuscript organization 5

3 State of the art **7**

3.1 Brake-by-Wire 7

3.1.1 Electro-Hydraulical Brakes (EHB) 8

3.1.2 Electro-Mechanical Brakes (EMB) 9

3.1.3 Comparison between EHB and EMB 12

3.2 Choice of Brake-by-Wire system 14

4 Modeling of Brake By Wire System **16**

4.1 Modeling of EMB Stand-alone System 16

4.1.1 DC Motor 17

4.1.2 Planetary gearbox 18

4.1.3 Ballscrew 19

4.1.4 Equation of motion 20

4.1.5 Friction model 20
4.1.6 Model summary 21
4.1.7 Control Logic 24
4.2 Integration of EMB within BEV model 27
4.2.1 Starting Vehicle Model 28
4.2.2 Vehicle Model Improvements 35
4.2.3 Parameters summary 42

5 Simulations and Results **44**
5.1 Simulations on EMB Model stand-alone 44
5.1.1 Step Input 5kN 45
5.1.2 Step Input 10kN 47
5.1.3 Step Input 15kN 50
5.1.4 Step Input 20kN 52
5.1.5 Discussions 54
5.2 Simulations on BEV Model 56
5.2.1 Simulation with UDDS cycle 57
5.2.2 Simulation with NYCC cycle 61
5.2.3 Simulation with UDDS cycle without regenerative braking . . 65
5.2.4 Discussions 70

6 Conclusions **73**

List of Figures

2.1 6 Levels of Automation (figure from [37]) 3

3.1 Brake by wire Scheme (figure from [38]) 7
3.2 Electro-hydraulic brake structure (Figure from [14]) 9
3.3 Electro-Mechanical Brake Structure (Figure from [14]) 10
3.4 Radar Diagram EHB vs EMB 13

4.1 EMB Scheme (Figure from [39]) 16
4.2 Dc Motor equivalent Circuit 17
4.3 Planetary Gearbox (Figure from [33]) 18
4.4 Ballscrew Stiffness Curve 20
4.5 Friction Model 21
4.6 EMB Plant Model 22
4.7 Cascade PID Control 24
4.8 Control logic implemented in Simulink 25
4.9 Example of Optimization Toolbox 26
4.10 Example of Optimization Toolbox 26
4.11 Starting Vehicle Model 28
4.12 Driver Subsystem Model 29
4.13 Brakes Subsystem Model 29
4.14 Motor Subsystem Model 31
4.15 Motor Torque Limiter block 32
4.16 Regen Torque Limiter block 32

4.17 Motor Power Losses 32
4.18 Battery Subsystem Model 33
4.19 Current Calculation 33
4.20 Driveline Subsystem Model 34
4.21 Glider Subsystem Model 35
4.22 Open Circuit Voltage of LiFePO4 36
4.23 Improved Battery Subsystem 37
4.24 Brakes Scheme 38
4.25 Estimation of deceleration rate 38
4.26 Improved Brake Subsystem 41

5.1 Clamping force 45
5.2 Motor speed 46
5.3 Current 46
5.4 Voltage 47
5.5 Clamping force 48
5.6 Motor speed 48
5.7 Current 49
5.8 Voltage 49
5.9 Clamping force 50
5.10 Motor speed 50
5.11 Current 51
5.12 Voltage 51
5.13 Clamping force 52
5.14 Motor speed 52
5.15 Current 53
5.16 Voltage 53
5.17 Clamping force and percentage bands 55
5.18 Speed Cycles 56
5.19 UDDS Vehicle Speed 57
5.20 UDDS Speed Error 58
5.21 UDDS Brake Force Demand 59

5.22 UDDS SOC 59
5.23 UDDS Zoom on vehicle speed and brake force demand 60
5.24 UDDS Zoom on current and SOC 60
5.25 UDDS Zoom on friction braking force and clamping force 61
5.26 NYCC Vehicle Speed 62
5.27 NYCC Speed Error 62
5.28 NYCC Brake Force Demand 63
5.29 NYCC SOC 63
5.30 NYCC Zoom on vehicle speed and brake force demand 64
5.31 NYCC Zoom on current and SOC 64
5.32 NYCC Zoom on friction braking force and clamping force 65
5.33 UDDS Vehicle Speed 66
5.34 UDDS Speed Error 66
5.35 UDDS Brake Force Demand 67
5.36 UDDS SOC 67
5.37 UDDS Zoom on vehicle speed and brake force demand 68
5.38 UDDS Zoom on friction braking force and clamping force 69
5.39 SOC variations 70

List of Tables

4.1 EMB Parameters Summary 23
4.2 PID Parameters Summary 27
4.3 Vehicle Parameters Summary 42

5.1 EMB Step Input Results 55
5.2 Speed Cycles Result Summary 71

Chapter 1

Abstract

In recent years, the evolution of autonomous vehicles has led to a growing interest in advanced braking systems, such as brake-by-wire (BBW), which offer significant advantages in terms of efficiency, safety, and maintenance. This thesis focuses on the modeling and simulation of a brake-by-wire (BBW) system using the MATLAB and Simulink environment. The main objective of this thesis is to develop a detailed model of the BBW system, based on electromechanical brakes (EMB), design an advanced control strategy, and integrate this into a BEV model, validating the system through simulations. The adopted methodology initially includes the design of the EMB system, with the creation of an accurate mathematical model of its main components, including the electric motor, the actuation system, and the control electronics. Subsequently, the EMB model is integrated into a complete BEV model to simulate the system's response to various operating conditions, accurately representing the vehicle's dynamic behavior. A rule-based control strategy, capable of understanding braking intensity, is developed to ensure the distribution of braking demand between the EMB system and regenerative braking. The results obtained demonstrate that the proposed model can faithfully replicate the dynamics of the BBW system. Furthermore, the implemented control strategy allows for battery SOC savings. In conclusion, this thesis contributes to the understanding and development of BBW systems for battery electric vehicles. The results obtained have potential implications for future research and applications in the field of advanced braking systems for electric vehicles.

Chapter 2

Introduction

2.1 Context

The rapid advancement of sustainable scientific research in the 21st century has profoundly impacted the transportation sector, giving rise to concepts such as smart mobility and autonomous vehicles (AVs). Smart mobility introduces an innovative concept of transportation, focused on the use of advanced technologies, innovative infrastructure, and data analysis to create an efficient and sustainable transportation system. To achieve this, smart mobility leverages "intelligent transportation systems (ITS), real-time traffic management, and shared mobility solutions, all aimed at enhancing urban mobility and reducing environmental impacts" [1]. Autonomous vehicles are a key component in the realization of smart mobility. These vehicles utilize various technologies such as sensors, artificial intelligence, real-time data analysis, and vehicle-to-everything (V2X) communication to perceive their surroundings and operate efficiently and safely without human control. "The adoption of AVs promises to significantly improve road safety by reducing accidents caused by human error, which accounts for the majority of traffic incidents". [2] Additionally, "AVs can optimize traffic flow and reduce congestion, contributing to more efficient urban transportation networks". [3] According to SAE International J3016-Standard, there are 6 levels of autonomous driving, ranging from no automation, level 0 and full automation, level 5. To achieve the level of full automation, which remains the focus of numerous ongoing research efforts, where "the system is capable of guiding

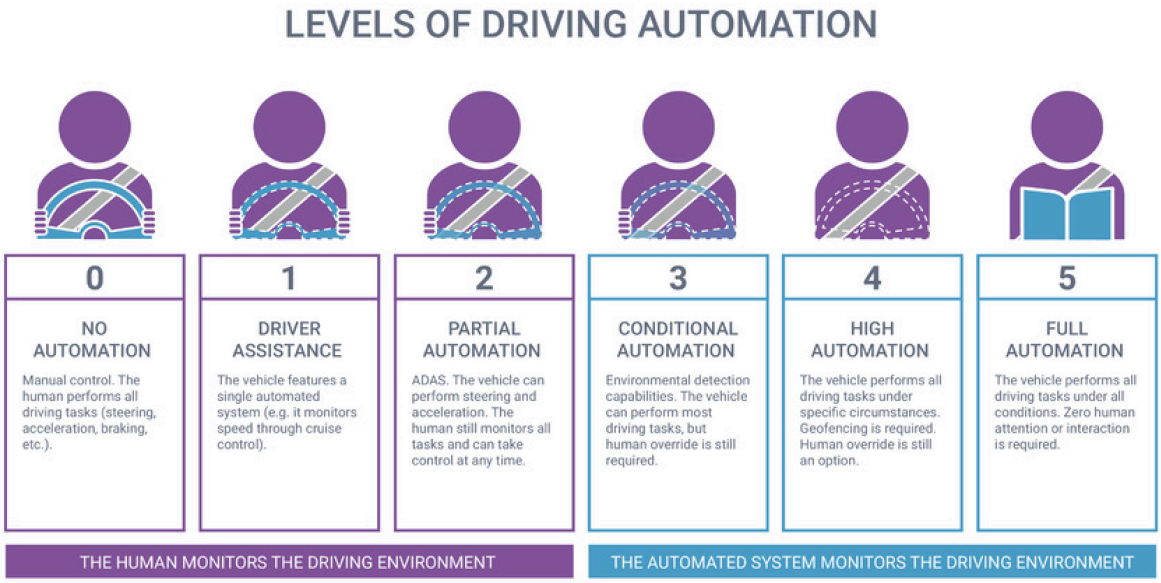

Figure 2.1: 6 Levels of Automation

(figure from [37])

the vehicle throughout complete trip, regardless of the starting and ending points or intervening road, traffic and weather condition" [4], drive by wire (X-By-Wire) technologies are essential components in autonomous vehicles. These technologies replace traditional mechanical control with more precise electronic control, thereby enhancing reliability and ensuring faster and more accurate responses, which are crucial for vehicle safety and performance. [5] The main drive-by-wire systems currently developed and studied include brake-by-wire, throttle-by-wire, steer-by-wire, shift-by-wire, and so on. Among the DBW technologies, for the purpose of this thesis, particular attention has been focused on brake-by-wire.

2.2 Scope of the thesis

Teoresi, "an engineering consultancy company with a focus on the automotive and telecommunications sectors," [6] is currently collaborating with XEV on autonomous driving applications. The purpose of this thesis, carried out in collaboration with the aforementioned company, is to create a digital model of brake-by-wire, applied to battery electric vehicles (BEVs). Specifically, the created digital platform must be able to replicate the behavior of the vehicles in specific situations, allowing for the evaluation of dynamic parameters related to the braking system and the vehicle, as well as energy parameters. For the development of the model, MATLAB and Simulink software were used, thanks to the "powerful computational tools they provide" [7], which are "widely used in the industry to model and simulate complex systems in various domains" [7].

2.3 Manuscript organization

In Chapter 3, an overview of the different brake-by-wire systems is provided, along with a comparison between them. In Chapter 4, a model of brake-by-wire is proposed initially as a stand-alone system and subsequently integrated into a BEV (Battery Electric Vehicle) model. In Chapter 5, simulations and results obtained from the implemented models are reported. Finally, in Chapter 6, a brief summary of the work done and future developments is provided.

Chapter 3

State of the art

3.1 Brake-by-Wire

Brake-by-wire (BBW) technology marks a major leap forward in automotive engineering, substituting traditional mechanical and hydraulic braking systems with electronic controls. In a brake-by-wire system, sensors detect the driver's brake pedal inputs and relay them to electronic control units (ECUs). The ECUs then actuate the brakes using electric motors or hydraulic actuators. This configuration eliminates the necessity for mechanical linkages and hydraulic fluid, offering several key advantages.

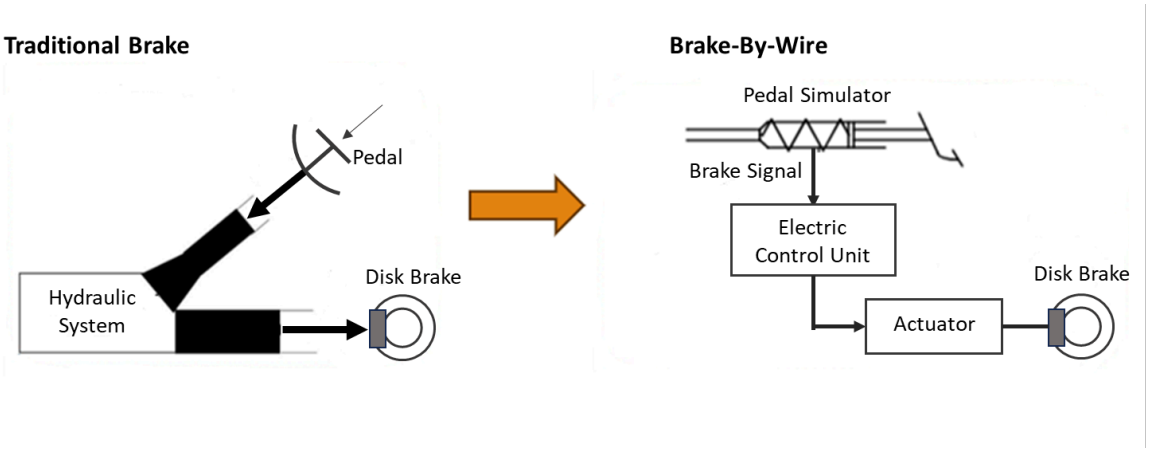

Figure 3.1: Brake by wire Scheme
(figure from [38])

By utilizing electronic signals "brake-by-wire systems can deliver faster and more accurate braking responses, which is crucial for the safety and performance of modern vehicles, especially in autonomous driving applications". [8] Additionally, these systems "can be easily integrated with other electronic control systems, such as stability control and advanced driver assistance systems (ADAS), providing a more cohesive and efficient vehicle control architecture". [9] Furthermore, BBW technology contributes to overall vehicle weight reduction, thereby enhancing fuel efficiency, handling, and performance." The modular nature of brake-by-wire systems also allows for easier maintenance and scalability, making them suitable for a wide range of vehicle types, from conventional cars to fully autonomous vehicles ". [10] Research indicates that brake-by-wire systems also play a significant role in the electrification of vehicles, particularly in electric and hybrid vehicles, where traditional braking systems are less efficient [11]. The regenerative braking capabilities of brake-by-wire systems enhance energy recovery and contribute to extended vehicle range [12]. This feature is particularly important as the automotive industry moves towards more sustainable and eco-friendly solutions. Depending on the actuator, the brake by wire system can be classified into two categories:

- Electro-Hydraulic Brake system (EHB)
- Electro-Mechanic Brake system (EMB)

3.1.1 Electro-Hydraulical Brakes (EHB)

Electro-hydraulic brakes (EHB) represent a cutting-edge advancement in automotive braking technology by integrating the precision of electronic controls with the robust power of hydraulic actuation. Unlike traditional brakes, which rely solely on mechanical linkages and hydraulic fluid to transmit the driver's input to the brakes, electro-hydraulic brake (EHB) systems use electronic sensors and control units to determine and regulate the braking process.[12] Figure 3.2 shows the structure of an EHB. The main components of the hydraulic actuators include high pressure accumulator, high pressure pump, high and low pressure oil pipes, solenoid valves (inlet and outlet valves) and so on, while the electronic control system includes sensors and electronic control unit (ECU). [13]

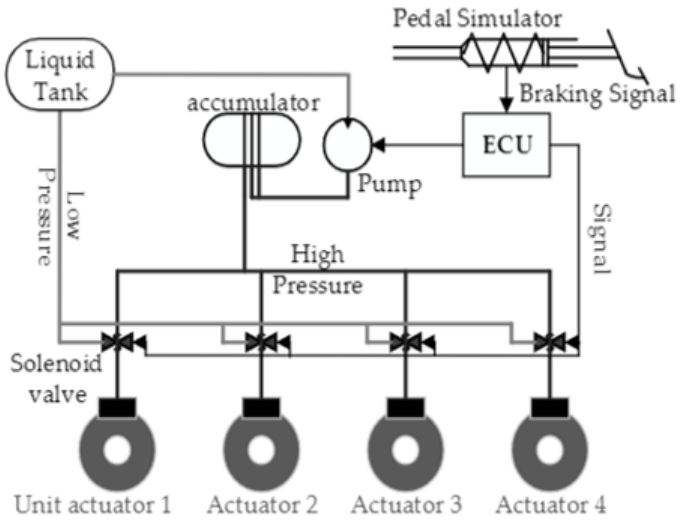

Figure 3.2: Electro-hydraulic brake structure
(Figure from [14])

During the braking phase, the sensor on the brake pedal converts the pedal stroke into an electric signal and sends it to the ECU. The ECU processes the input from the pedal sensor along with data from other sensors (like vehicle speed, wheel speed, and ABS sensors). It calculates the necessary braking force required to safely stop the vehicle and sends a control signal to the electric motor. The electric motor drives the hydraulic pump, which pressurizes the hydraulic fluid stored in the reservoir. The ECU then commands the opening of the solenoid inlet valves, allowing the high-pressure fluid to travel through the brake lines to the brake calipers or wheel cylinders, thereby braking the vehicle. In absence of braking command, the ECU closes the inlet valves and opens the outlet valves, allowing the brake fluid to return from the wheel cylinder to the liquid reservoir. [15][16] In this way, the direct mechanical connection between the brake pedal and the braking system is eliminated. In traditional systems, this connection provides the driver with a direct and intuitive feel of the brake behavior. To maintain this sensation in EHB systems, a brake pedal simulator is used.[17]

3.1.2 Electro-Mechanical Brakes (EMB)

Electro-mechanical brakes (EMB) are a type of braking system that uses electrical energy to directly actuate the mechanical braking components. This system eliminates

the need for hydraulic fluid and the associated components found in traditional and electro-hydraulic brake systems, achieving "dry brake by wire". [18] The absence of hydraulic components allows for benefits in terms of high transmission efficiency, environmental protection, and energy saving.[19] Figure 3.3 shows the structure of an EMB. The main components of an Electro-Mechanical Braking (EMB) system include electric motor, torque amplyifing mechanism, rotatory-to-linear motion conversion mechanism and various sensors.

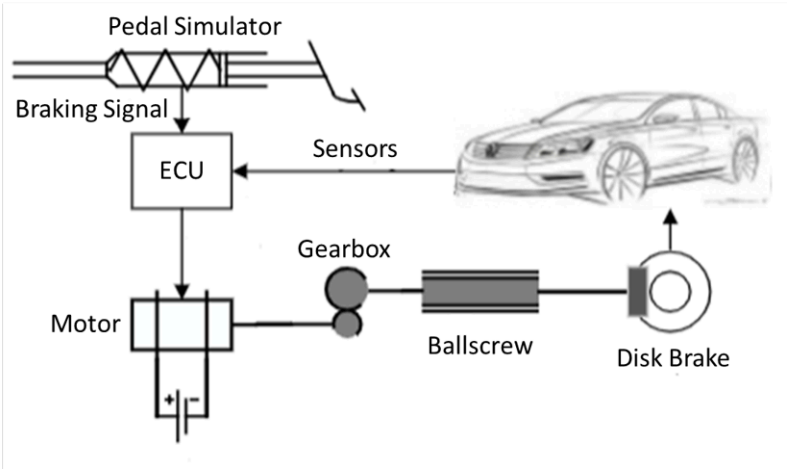

Figure 3.3: Electro-Mechanical Brake Structure
(Figure from [14])

The operating principle of an electro-mechanical brake (EMB) system, can be explained as follows:

- Brake Pedal Pressure: when the driver presses the brake pedal, a sensor detects the pedal stroke.
- Signal to ECU (Electric Control Unit): The sensor sends an electrical signal proportional to the pedal pressure to the Electronic Control Unit (ECU). The latter processes the signal received from the pedal sensor, integrating information from other sensors to determine the necessary braking force.
- Activation of the motor: The ECU sends a command to the electric motor of the braking unit, which is responsible for generating the necessary force to brake.
- Amplification of torque: The torque generated by the motor is amplified through an amplification mechanism.

- Transformation of motion from rotary to linear: The rotary motion is converted into linear motion through a mechanism.
- Application of Braking Force: The linear motion pushes the brake pad against the brake disk. This contact generates friction, which produces the necessary braking force to slow down or stop the vehicle.

In absence of braking command, the ECU reverse the motion of the motor, which drives the motion conversion mechanism to its original position. Similarly to EHB, in these systems, a brake pedal simulator is also necessary to ensure the driver experiences sensations similar to those of traditional hydraulic brakes. Despite the fact that EMBs are not currently available on commercial vehicles, their significant potential has attracted the interest of several manufacturers. The main researches mainly focus on both the structure and the control logic adopted. In this regard, Bosch GMBH, Continental AG , and Mando Corporation have proposed an actuator structure consisting of a planetary gearbox as a torque amplification mechanism and a ballscrew for motion conversion.[20][23][24][25] Similar solutions have been presented by Siemens and Continental AG, where the force amplification mechanism utilizes the wedge self-energizing mechanism.[21][22]
The main control strategies for Electro-Mechanical Brakes (EMB) include two primary methods: direct control and indirect control of the clamping force exerted by the brake pad on the brake disk. Direct control uses closed-loop control on the clamping force, receiving feedback signals via load cell, position sensor, and current sensor ensuring high precision, rapid response, and continuous feedback. The main algorithm used is PID control for its simple structure and ease of application. [26][27] Other strategies include the use of H-infinity control for achieving greater stability, sliding mode control, and various other algorithms.[28][29][30] On the other hand, indirect control uses mathematical models and algorithms to estimate the clamping force and adapt actuators accordingly, thereby eliminating the high costs associated with the load cell. The estimation can be based on the motor angular displacement, current, or a fusion of both. [20][31]

3.1.3 Comparison between EHB and EMB

While both EHB and EMB offer braking capabilities with advanced electronic control, they differ significantly in terms of technology, energy efficiency, maintenance requirements, and environmental impact. The choice between the two depends on factors such as application requirements, cost considerations, and desired performance characteristics. EHB systems are known for their ability to deliver high braking force through hydraulic pressure, making them ideal for heavy-duty applications requiring strong braking power. They utilize established technology from hydraulic brake systems, integrating electronic control for advanced functionality and improved safety. EHB systems provide a smoother braking feel, which is particularly beneficial when precise modulation of braking force is necessary. They are adaptable and can be easily integrated with existing hydraulic brake systems, whereas integrating EMB systems into vehicles requires a complete modification of the braking system. On the other hand, EMB systems are known for their superior energy efficiency by eliminating the need for hydraulic fluids for pressurization and distribution. They offer precise control of braking force through electronic actuators, potentially allowing for faster response times compared to EHB systems. EMB systems require less maintenance than EHB systems since they do not involve managing hydraulic fluids and are less susceptible to fluid leaks or seal wear. By eliminating hydraulic components and utilizing compact electronic actuators, EMB systems are lighter and less complex than EHB systems. They are considered more environmentally friendly by eliminating hydraulic fluids, thus reducing environmental impact and risks associated with fluid leaks or disposal. Additionally, EMB systems typically incur higher initial costs compared to EHB systems due to the presence of expensive components such as load cells, although these costs are expected to decrease with economies of scale. The figure 3.4 summarizes the above information in a radar chart, assigning a rating from 1 to 5 for each category for the two types of brakes.

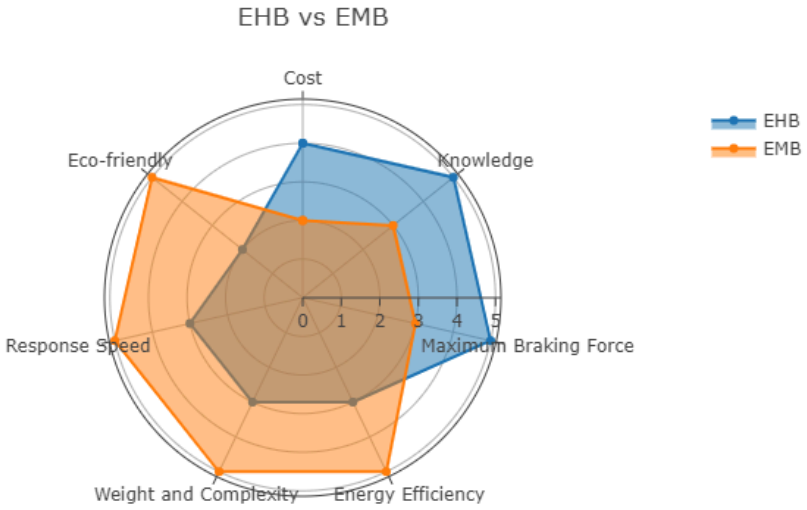

Figure 3.4: Radar Diagram EHB vs EMB

3.2 Choice of Brake-by-Wire system

For autonomous vehicles, it is crucial to use precise and responsive systems to ensure vehicle safety. As explained in paragraph 3.1.3, EMB systems best meet these requirements. For application in small, lightweight battery electric vehicles, such as the XEV YOYO, where high braking force is not required, EMBs can be a significant breakthrough in terms of dynamic and energy performance. Additionally, from a sustainable research perspective, the possibility of using a more eco-friendly system can be a major drive for further development and application of these systems in vehicles. For these reasons, EMB brakes were selected for the implementation of the brake-by-wire model in Simulink.

Chapter 4

Modeling of Brake By Wire System

The modeling of the brake-by-wire system was carried out in two steps: first, it was necessary to create an appropriate model of the EMB brake, and subsequently, this was applied to a model of a battery electric vehicle (BEV).

4.1 Modeling of EMB Stand-alone System

Despite the numerous solutions available for electro-mechanical brakes, the main configuration selected in this manuscript includes the use of a DC motor, a planetary gearbox as a force amplification mechanism, and a ballscrew for transforming the motion from rotary to linear.

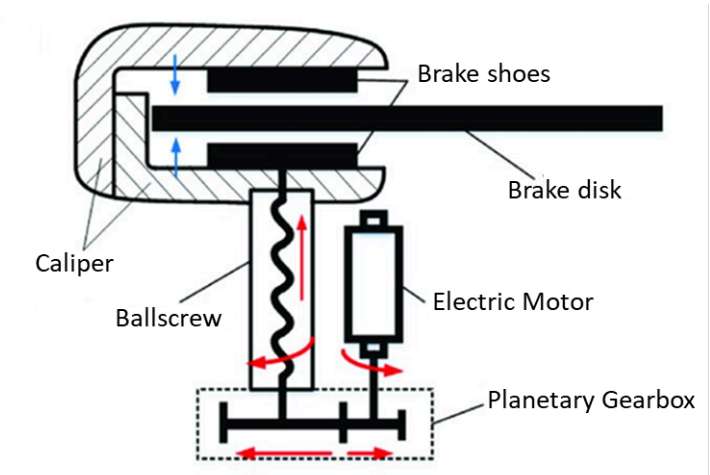

Figure 4.1: EMB Scheme
(Figure from [39])

For the creation of the model , it was necessary to describe each fundamental component of the system and subsequently use an appropriate control logic capable of meeting the dynamic requirements characteristic of braking.
To simplify the system modeling in Simulink, the following assumptions have been made:

- The system model represents half of the caliper, assuming that the force applied to one brake pad is equal to the reaction force exerted by the other brake pad. This neglects the real case where one brake pad makes contact with the disc before the other.
- When the brake is released, the brake pads completely detach from the disc, thus neglecting any possible residual drag.
- For stiffness modeling, the hysteresis phenomenon is neglected.

4.1.1 DC Motor

The description of the electrical part of the DC motor concerning the armature voltage, current, and back electromotive force requires the definition of an equivalent circuit shown in the following figure.

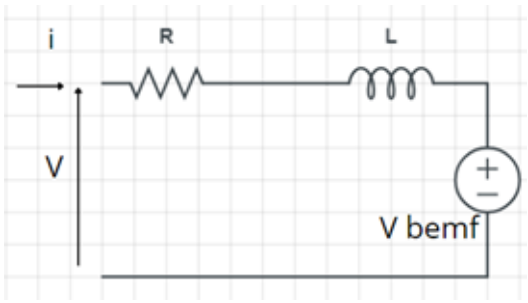

Figure 4.2: Dc Motor equivalent Circuit

The characteristic equation of the circuit 4.2 is as follows:

$$V_q(t) = Ri_q(t) + L\frac{di_q(t)}{dt} + V_{bemf} \tag{4.1.1}$$

Where L represents the inductance, assuming the motor has only one polar termination, R represents the resistance of the electrical circuit, and V_{bemf} the back

electromotive force. The following fundamental relationships also hold true:

$$T_m(t) = k_t i_q(t) \tag{4.1.2}$$

$$V_{bemf} = k_e \frac{d\dot{\theta}}{dt} \tag{4.1.3}$$

In 4.1.2, the torque generated by the motor depends on the motor's characteristic constant,k_t, and on the supplied current. In 4.1.3, the back electromotive force is a function of the motor angular speed.
The voltage V_q applied to the terminals of the motor armature generates a current, which in turn is responsible for the torque generated by the electric motor. To achieve the required value of mechanical torque, the voltage V_q is appropriately regulated.

4.1.2 Planetary gearbox

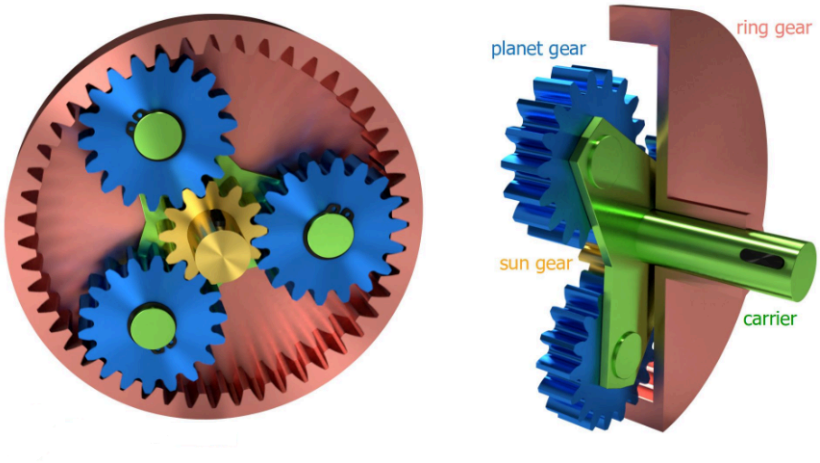

Figure 4.3: Planetary Gearbox (Figure from [33])

To describe the behavior of the planetary gearbox, the Willis formula was considered:

$$n_r z_r = n_c(z_r + z_s) - z_s n_s \tag{4.1.4}$$

where the subscripts represent the different components; s refers to the sun gear, r to the ring gear, and c to the carrier, while z and n represent respectively the number of teeth and the rotational speed. As explained previously, the use of this component is crucial for torque amplification. Therefore, the operation for this application involves

fixing the ring gear so that the motion enters through the sun gear and exits through the carrier. The equation 4.1.4 thus becomes:

$$N_1 = \frac{n_c}{n_s} = \frac{z_s}{z_s + z_r} \tag{4.1.5}$$

Where N_1 is the gear ratio of the gearbox.

4.1.3 Ballscrew

The mechanism used to convert rotary motion, output of the planetary gearbox, to linear motion is the ballscrew. The relationship between linear displacement and angular displacement is as follows:

$$x = N_2 \theta_c \tag{4.1.6}$$

where N_2 represents the transmission ratio, expressed in $[\frac{mm}{rev}]$, x is the linear displacement and θ_c is the angular displacement.
For an appropriate modeling of the EMB, the modeling of the ballscrew stiffness curve is of particular importance. The stiffness curve which links the ballscrew displacement to the clamping force, is proven to be a third-degree polynomial function[34].

$$F_{cl} = A_1 x^3 + A_2 x^2 + A_3 x + A_4 \tag{4.1.7}$$

Thus, the stiffness curve obtained from empirical data [30] is expressed as:

$$\left[\begin{array}{rl} F_{cl} = -7.23x^3 + 33.7x^2 - 3.97x & \forall x > 0.125 \\ F_{cl} = 0.1295x & \forall x \leq 0.125 \end{array} \right] \tag{4.1.8}$$

where F_{cl} is express in $[kN]$ and x in $[mm]$

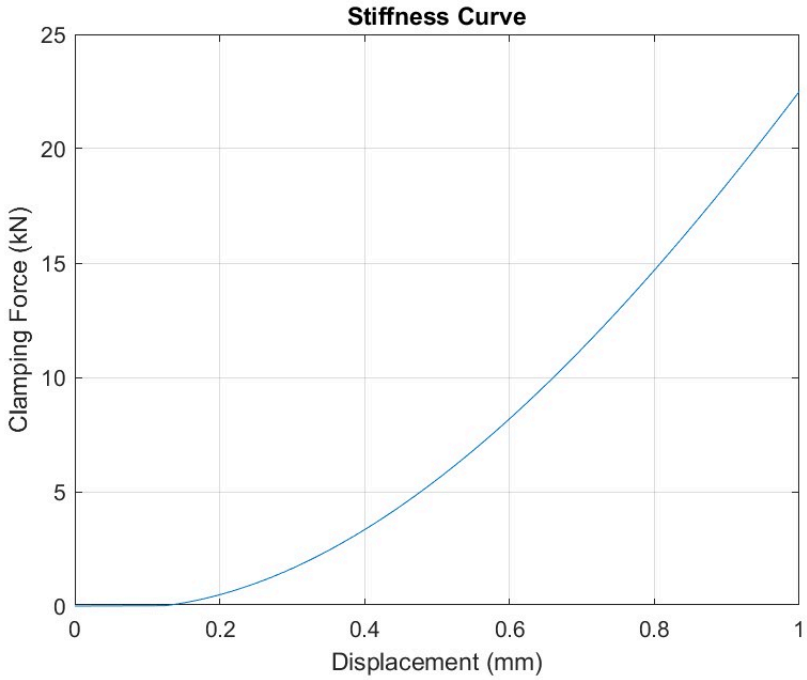

Figure 4.4: Ballscrew Stiffness Curve

Graphically, the stiffness curve is shown in 4.4.
The 0 value represents the contact point between the brake pad and the brake disc.

4.1.4 Equation of motion

To describe the motion equation of the system, it was considered a torque balance on the motor shaft:

$$T_m = J\ddot{\theta} + T_F + T_{load} \tag{4.1.9}$$

where J is the total inertia of the system, T_F is the torque generated from friction and T_{load} is the load torque due to the clamping force.

Using 4.1.2, the motion equation becomes:

$$k_t i - T_F - F_{cl} N = J\ddot{\theta} \tag{4.1.10}$$

where $N = N_1 N_2$ is the total transmission ratio.

4.1.5 Friction model

To describe the friction, a classic friction model including Coulomb, viscous, and static friction was considered.[35]

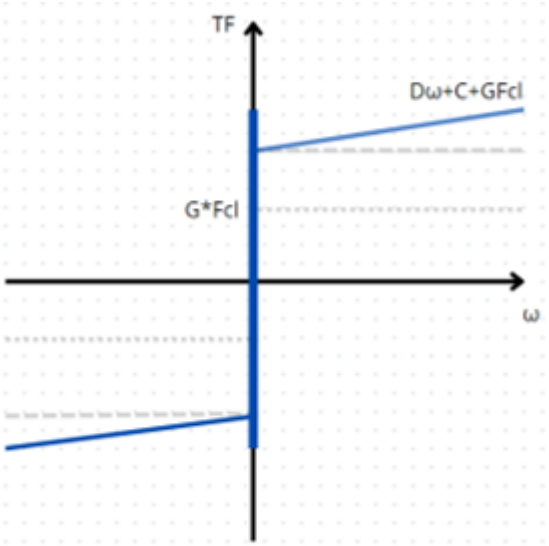

Figure 4.5: Friction Model

Since the friction of the system is influenced by the clamping force, an additional term accounting for this dependency was also added, as shown in 4.5.
The friction torque can be expressed as a function of speed, clamp load and external torque:

$$T_F = T_F(\dot{\theta}, T_E, F_{cl}) \tag{4.1.11}$$

$$\begin{bmatrix} T_F = D\dot{\theta} + (C + GF_{cl})sign(\dot{\theta}) & \forall \left|\dot{\theta}\right| > 00 \\ T_F = T_e & \forall \left|\dot{\theta}\right| = 0 \wedge |T_e| < (T_s + GF_{cl}) \\ T_F = (T_s + GF_{cl})sign(T_e) & otherwise \end{bmatrix} \tag{4.1.12}$$

Where D is the vicous friction coefficient, C is the Coulomb friction torque, T_s is the static friction torque and G is the load-dependency coefficient.

4.1.6 Model summary

The plant model implemented in Simulink is shown.

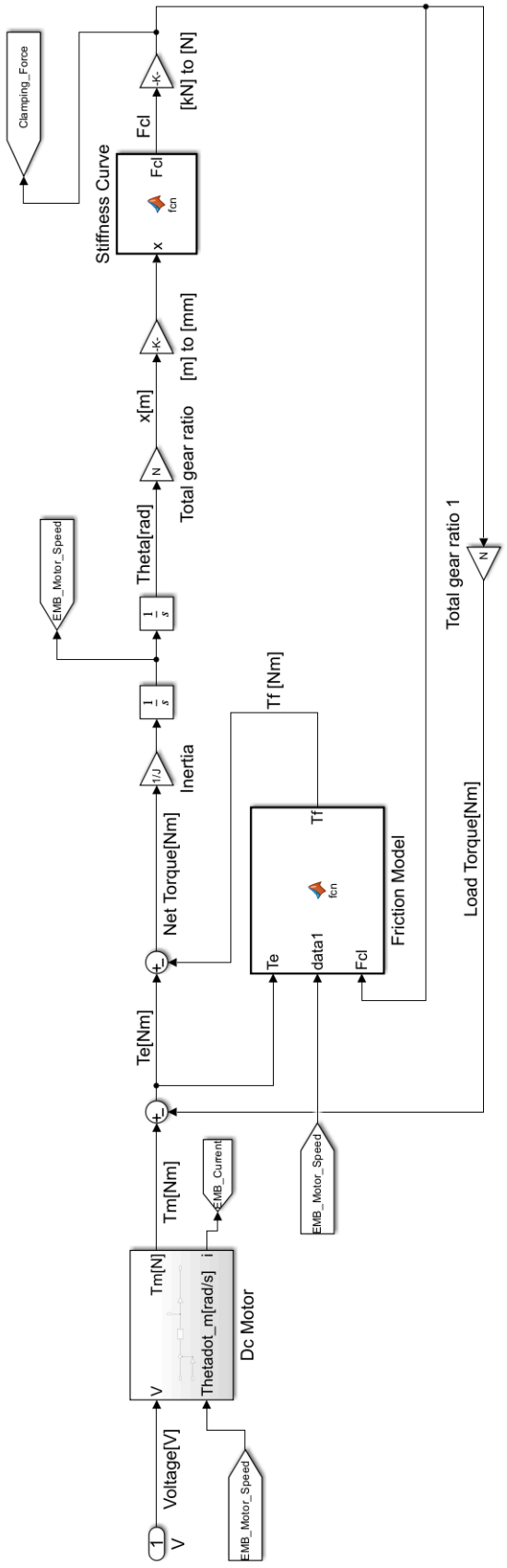

Figure 4.6: EMB Plant Model

Table 4.1: EMB Parameters Summary

J	0.310	kgmˆ2	Total Inertia
N	2.63*10ˆ-7	m/rad	Total Gear Ratio
L	2.5*10ˆ-3	H	Motor Inductance
R	1	Ohm	Motor Resistance
Kt	0.13	Nm/A	Motor Torque Constant
Ts	0.027	Nm	Static Friction Torque
C	0.0304	Nm	Coulomb Friction Torque
D	3.95*10ˆ-4	Nms/rad	Viscous friction coefficient
G	1.17*10ˆ-5	Nm/N	Load-dependency coefficient

The input of the model is the voltage applied across the motor armature. Using the equations 4.1.1, the torque generated by the motor is obtained. As indicated in the motion equation 4.1.9, by subtracting the values of the friction torque and load torque and dividing by the total inertia of the system, the acceleration is obtained. The latter is then integrated to obtain the motor's rotational speed, $\dot{\theta}$, and further integrated for motor angular displacement θ. Multiplying the angular displacement by the total gear ratio yields linear displacement x. Finally, using the stiffness curve 4.4, the clamping force, which is the output of the system, is determined. Additionally, as shown in figure 4.5, the values of friction torque and load torque are obtained using equations 4.1.12.

In the Table 4.1, the values used for modeling are summarized.

4.1.7 Control Logic

After developing the EMB model, it was necessary to implement a control logic to effectively manage the clamping force. Among the control strategies for EMBs investigated, PID control was chosen for its simple structure and good adaptability. Since the braking process of a vehicle is critical to ensure safety, a cascade PID control with three close-loop was used. Although the cascade PID loop is more complex than the single PID loop, this added complexity can improve control performances and disturbance rejection which may occur in vehicles application. The following figure shows a diagram of the implemented control logic.

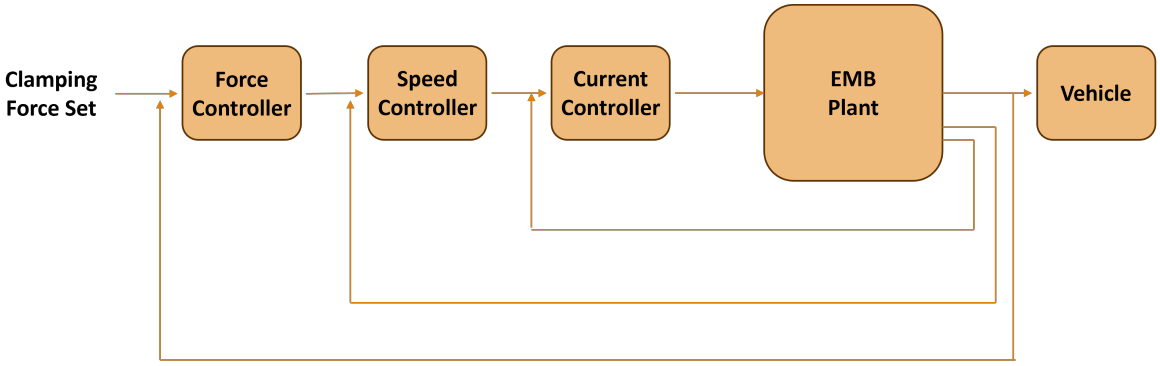

Figure 4.7: Cascade PID Control

The cascade control can be described as a series of three steps:

- The outermost loop is used to accurately track the set clamping force value by regulating the motor speed.
- The intermediate loop is necessary to track the motor speed set, obtained from the previous loop, by regulating the motor current.
- Finally, the innermost loop tracks the set current by regulating the voltage applied to the electric motor, input of the EMB plant.

Using the previously described logic, the control logic implemented in Simulink logic is shown.

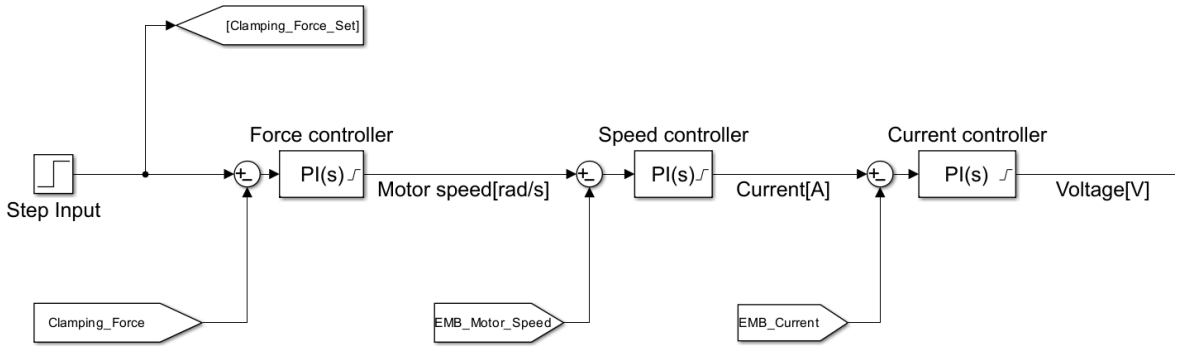

Figure 4.8: Control logic implemented in Simulink

As can be seen in 4.8, saturation values reflecting limitations of EMB components were considered for each of the PID controllers:

- The maximum motor rotation speed is 350 rad/s.
- To prevent motor overheating, the maximum current value is ±25A
- The maximum voltage applied to the motor is ±42V.

Tuning of PID Controller Parameters

The complexity of a cascade PID control lies primarily in tuning the parameters of each PID controller. This process requires a deep understanding of the system dynamics and interactions between the control loops.It often requires iterative adjustments and extensive testing to achieve optimal control performance. Utilizing the Simulink Optimization Toolbox for PID parameter characterization is an effective approach to optimize system performance. This tool enables defining desired performance objectives such as rise time, settling time, overshoot, and undershoot, and automating the parameter tuning process to minimize error between desired input and system response.

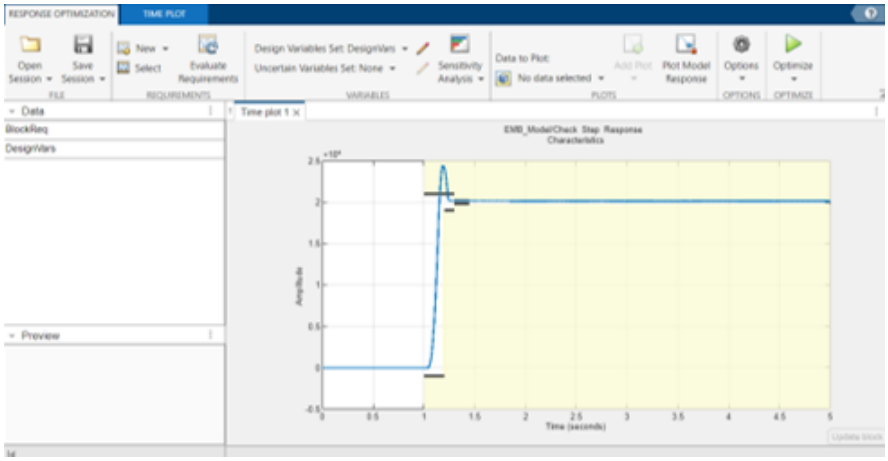

Figure 4.9: Example of Optimization Toolbox

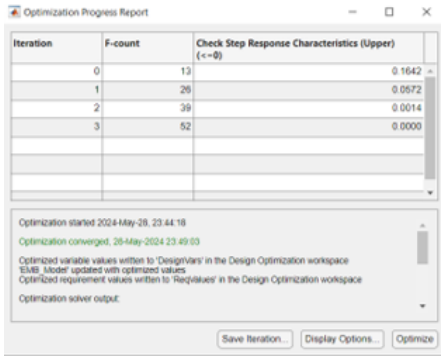

Figure 4.10: Example of Optimization Toolbox

In the figures 4.9 and 4.10, an example of using the Simulink Optimization Toolbox for PID parameter tuning is demonstrated. This allows visualizing optimization results and assessing how PID parameters influence system performance relative to predefined objectives. This approach can be particularly useful for expediting the PID tuning process and achieving better adaptability to specific system dynamics. However, it's essential to note that PID parameter optimization is an iterative process, and further manual adjustments were needed to attain the desired optimal performance across all operating conditions. The following table summarizes the values for the PID controllers:

Table 4.2: PID Parameters Summary

Force Controller P	0.0295
Force Controller I	4.7512*10^-5
Speed Controller P	1.2243
Speed Controller I	0.2985
Current Controller P	1.3478
Current Controller I	18.359

4.2 Integration of EMB within BEV model

The critical aspect of brake-by-wire (BBW) systems lies in determining the required braking force and ensuring that it is delivered as quickly as possible through the various actuators. Additionally, in particular for electric vehicles, regenerative braking is crucial for achieving greater efficiency. Consequently, an appropriate BBW system must include a braking distribution strategy that considers the braking intensity while ensuring vehicle safety. With these considerations, the next step was to integrate and test the EMB system in a model of a battery electric vehicle (BEV). To achieve this, a simple initial model was considered. Subsequently, various modifications were made to characterize the model and approximate it to that of a XEV YOYO. This process aimed to ensure that the integrated model accurately reflects the real-world dynamics and braking performance of the vehicle, providing a reliable basis for further analysis and optimization.

4.2.1 Starting Vehicle Model

The initial model considered is created using an equation approch and allows for the analysis of the behavior of an electric vehicle in exclusively longitudinal motion.

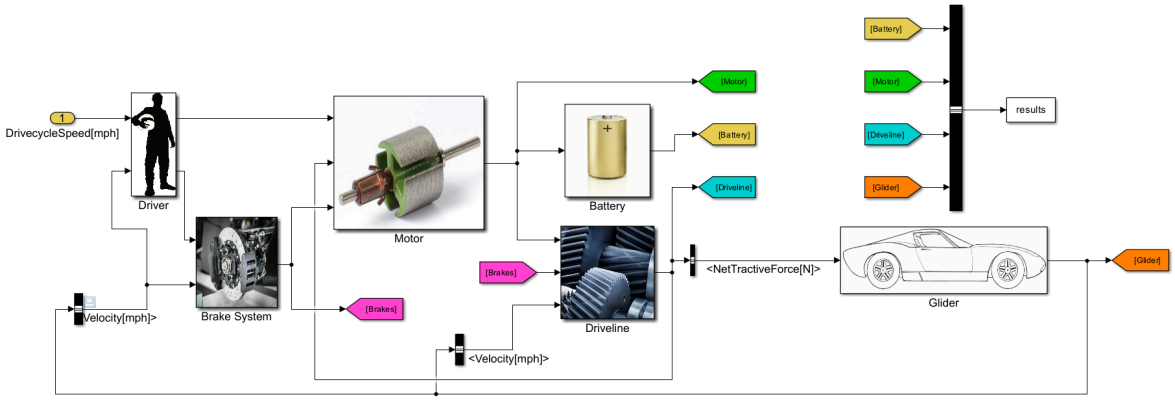

Figure 4.11: Starting Vehicle Model

The model, presented in figure 4.11, decomposes the vehicle into various subsystems, each representing the main components:

- Driver
- Brakes
- Motor
- Battery
- Driveline
- Glider

This model takes as input the reference speed from a known cycle, compares it with the vehicle speed calculated by the model, and based on the error, commands each subsystem to obtain the state of charge (SOC) and the vehicle's status,reflecting the performance and efficiency.

Driver Subsystem

The subsystem uses the error between the set speed and the calculated speed to determine an acceleration or deceleration command, each partialized in a range from 0-100% as shown in the following figure.

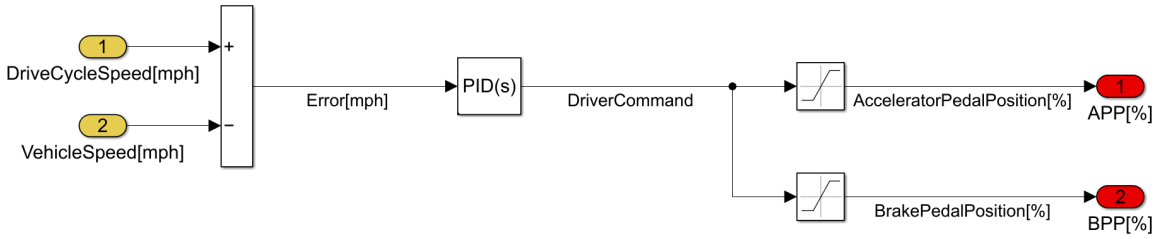

Figure 4.12: Driver Subsystem Model

Brakes Subsystem

The brake subsystem uses the brake pedal position (BPP) obtained from the driver subsystem to determine the braking force request. To do this, during the braking phase, the BPP value is multiplied by the maximum braking force that the system can deliver, which is set as a constant value in the model. Subsequently, the braking force request is divided into regenerative braking and friction braking using a constant factor. Additionally, if the vehicle speed is below a certain threshold value, braking is entirely managed by the friction brakes.

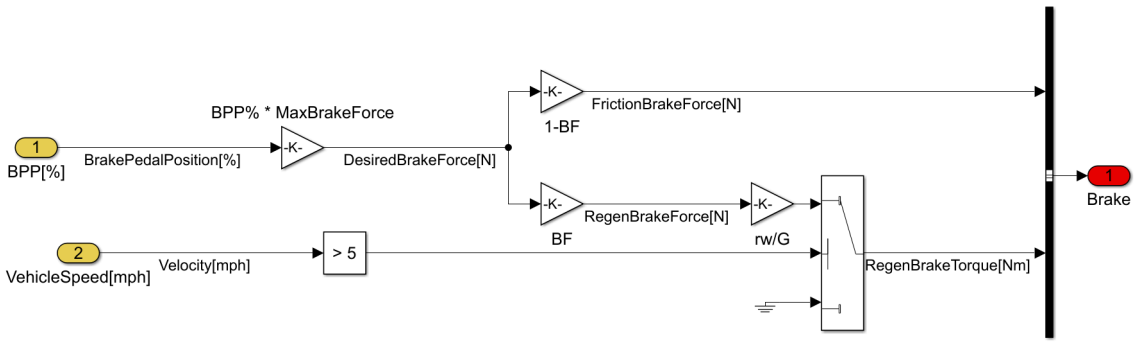

Figure 4.13: Brakes Subsystem Model

Motor Subsystem

The motor subsystem uses the acceleration command (APP), obtained from the driver subsystem, and the regenerative braking command, obtained from the brake subsystem, as inputs to determine the torque and power delivered by the motor. During acceleration, to determine the traction torque provided by the motor, the maximum torque and power output of the motor are considered, as indicated in equation 4.2.1.

$$m = \min[MaxTorque, \frac{MaxPower}{\omega_m}] \tag{4.2.1}$$

The lower value between these two is used to obtain the positive traction torque using equation 4.2.2.

$$T_P = APP * m \tag{4.2.2}$$

During the braking phase, in order to regenerate energy, the rotation of the electric motor is reversed, generating a braking torque, the maximum value of which depends closely on the specifications of the motor. To account for this, the maximum value is interpreted as a percentage of the maximum torque that the motor can deliver during traction, according to equation 4.2.3.

$$T_{All} = k * m \tag{4.2.3}$$

Referring to figures 4.14, during acceleration, the APP has a positive value while the regenerative braking command is zero, resulting in positive motor torque. During braking, the behavior is reversed, resulting in negative motor torque, thus slowing down the vehicle. Additionally, the value of power erogated from the motor and the power losses are obtained using the motor net torque. As shown in figure 4.17, motor power losses are calculated using the following equation:

$$k_c {T_{m\_net}}^2 + k_w {\omega_m}^3 + k_i \omega_m + C = P_{loss} \quad \forall \omega_m > 0 \tag{4.2.4}$$

where k_c, k_w, k_i and C are coefficients dependent on the motor specifications

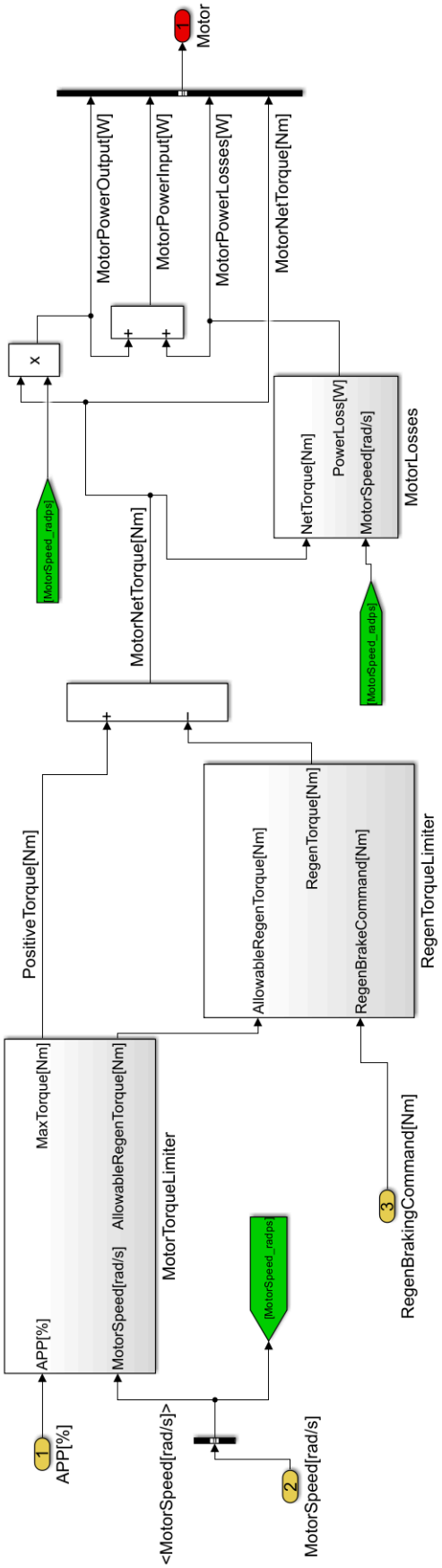

Figure 4.14: Motor Subsystem Model

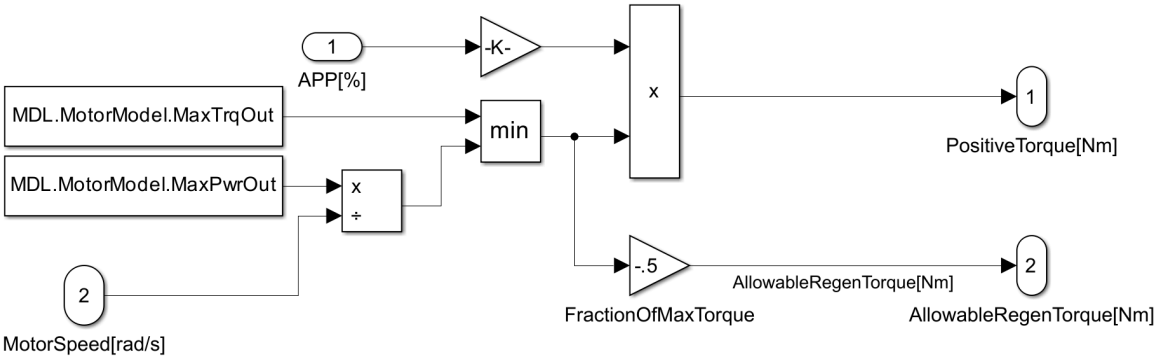

Figure 4.15: Motor Torque Limiter block

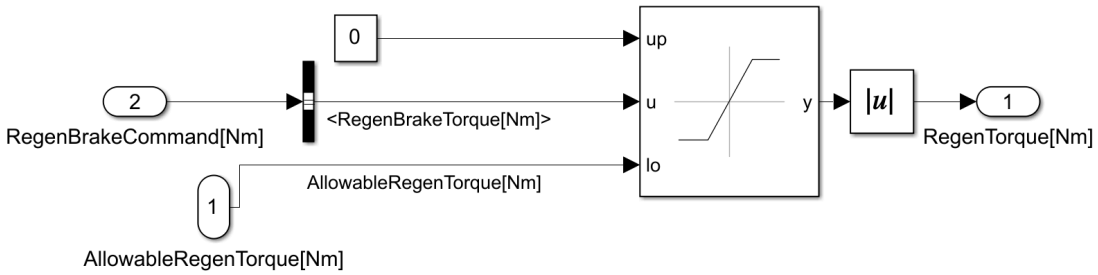

Figure 4.16: Regen Torque Limiter block

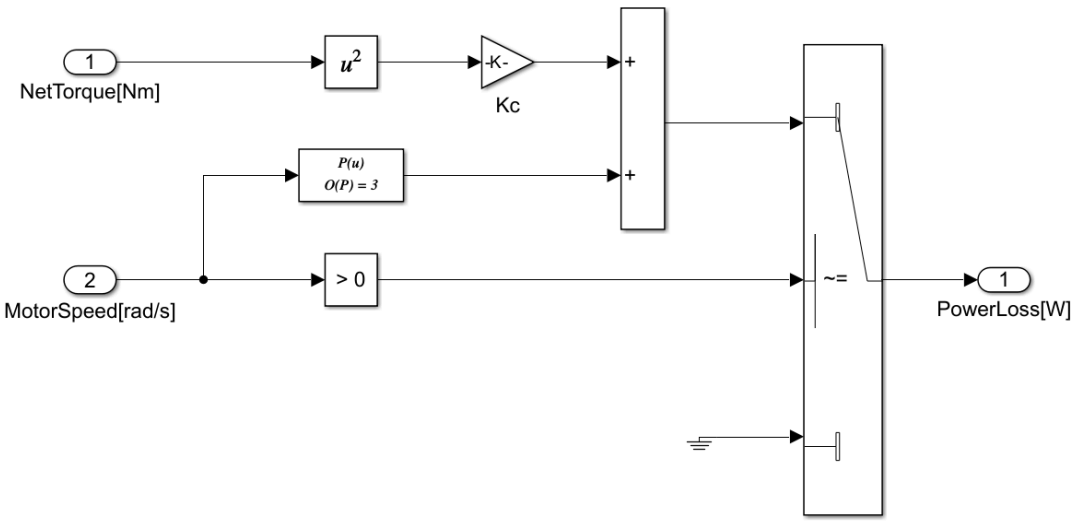

Figure 4.17: Motor Power Losses

Battery Subsystem

To characterize the behavior of the vehicle's battery, the model uses the equivalent circuit approach.

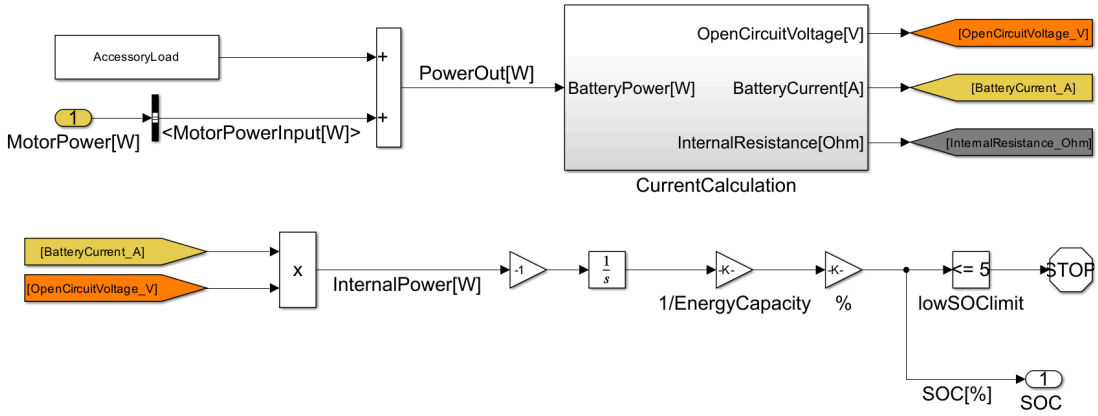

Figure 4.18: Battery Subsystem Model

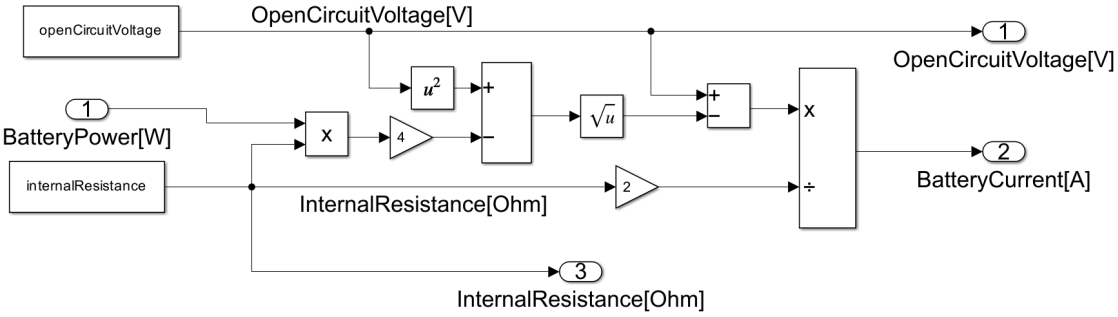

Figure 4.19: Current Calculation

As shown in figure 4.18, the model uses the power demanded by the motor and an accessory load to determine the current supplied by the battery. Referring to figure 4.19, the current is calculated using equation 4.2.5, where V_{OC} is the open circuit voltage and R is the internal resistance of the battery, both considered as constant values.

$$I = \frac{V_{OC} - \sqrt{{V_{OC}}^2 - 4RP}}{2R} \tag{4.2.5}$$

The state of charge (SOC) is determined using the following formula:

$$SOC = \frac{1}{Cap_{batt}} \int_0^t P_{int} \tag{4.2.6}$$

where Cap_{batt} is the battery capacity.

Driveline Subsystem

Using the traction torque provided by the motor and the braking force derived from the braking subsystem, the net force applied to the vehicle can be determined as follows:

$$F_{tr} = (T_m - T_{loss})\frac{G}{r_{wheel}} - F_{br} \tag{4.2.7}$$

where G is the transmission ratio of the driveline, T_{loss} are the torque losses of the driveline due to spin and r_{wheel} is the wheel radius of the vehicle. Referring to figure 4.20, during the acceleration phase, the torque delivered by the motor has a positive value, while the braking force is zero, resulting in a traction force. In the braking phase, the behavior is reversed, resulting in a braking force responsible for decelerating the vehicle.

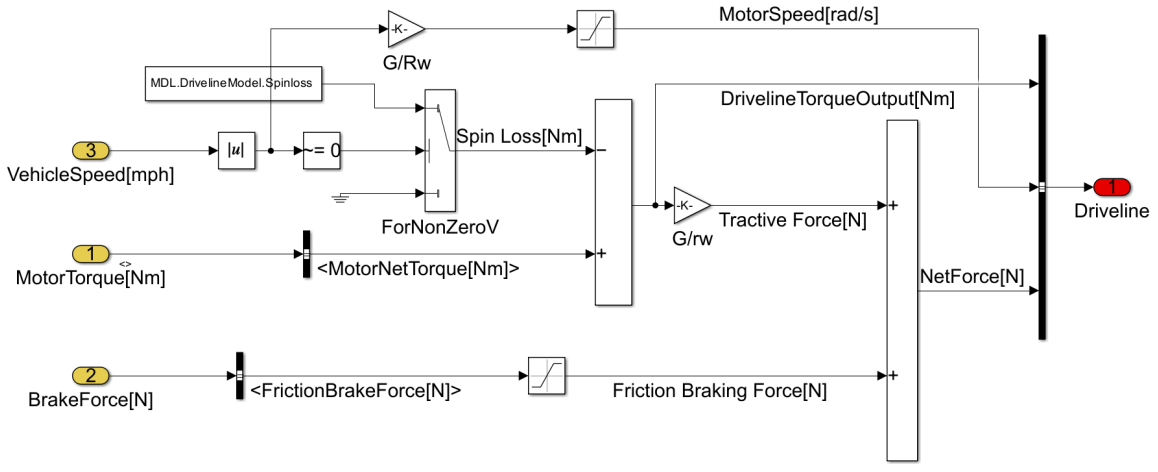

Figure 4.20: Driveline Subsystem Model

Glider Subsystem

Finally, using the net traction force and considering the forces acting on the vehicle:

$$F_{tr} = F_{aero} + F_i + F_{grade} + F_{rr} \tag{4.2.8}$$

where F_{aero}, F_i, F_{rr} and F_{grade}, are respectively the aerodynamic drag force, the inertial force, the rolling resistance force and the force due to the road incline. Substituting:

$$F_i = F_{tr} - \frac{1}{2}\rho_{air} C_D A - mg\sin(\vartheta) - mgC_{rr} \tag{4.2.9}$$

From 4.2.9, it's possible to obtain the acceleration and velocity of the vehicle.

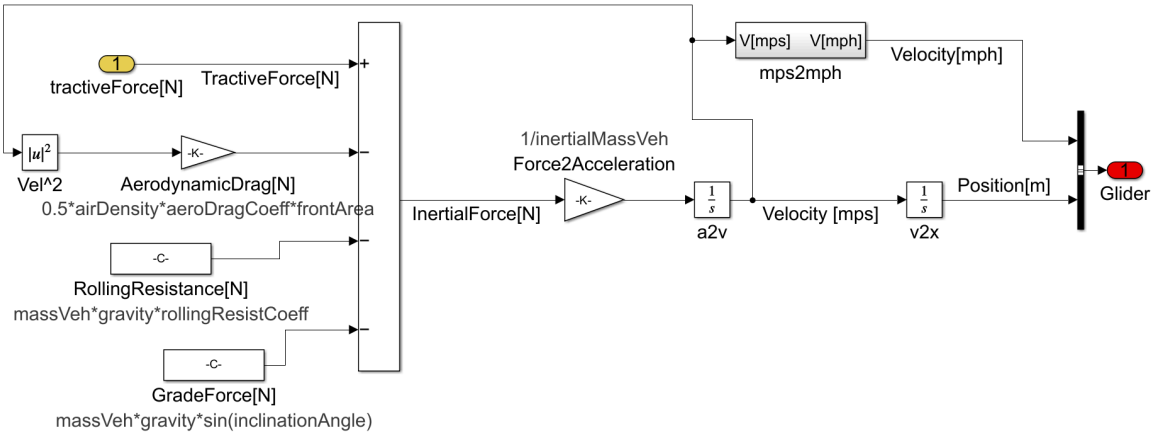

Figure 4.21: Glider Subsystem Model

4.2.2 Vehicle Model Improvements

In order to characterize the initial vehicle model and bring it closer to that of an XEV YOYO, several modifications have been implemented:

- Parameters of vehicle
- Changes on battery subsystem
- Changes on brake subsystem
- Other minor changes

Changes on battery subsystem

To improve the battery model and consider the real dynamics of a LiFePO4 battery, used in the XEV YOYO, the equivalent circuit approach was utilized. While in the previous model the Open Circuit Voltage (OCV) was considered constant,here, the OCV is depicted as a function of the State of Charge (SOC) of the battery. This relationship is crucial for accurately modeling the battery's behavior under different charge conditions. The OCV typically varies with the SOC, and capturing this variation helps in better predicting the performance and efficiency of the battery in the vehicle model.

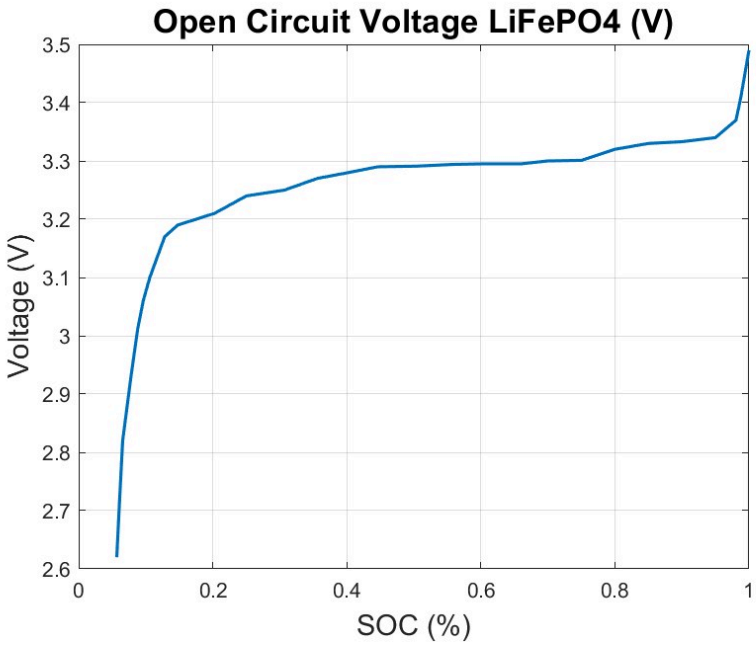

Figure 4.22: Open Circuit Voltage of LiFePO4

This function can be represented graphically or through a table that maps different SOC values to their corresponding OCV values as shown in 4.22 where the OCV of a LiFePO4 is depicted. Considering the battery as a combination of cells in series and parallel, the relationship for a single cell is:

$$V_T = V_{OC} - I_{batt} R_{int} \tag{4.2.10}$$

Where V_T is the voltage of the single cell and I_{batt} is the per model battery current. The per module battery current can be evaluated considering the number of cells in

parallel:

$$I_{batt} = \frac{I_{in}}{N_p} \tag{4.2.11}$$

The total battery voltage depend on the number of cell in series:

$$V_{out} = N_s V_T \tag{4.2.12}$$

Of particular importance is the State of Charge (SOC) of the battery, which is calculated using the following equation:

$$SOC(t) = SOC_0 - \frac{1}{Cap_{batt}} \int_0^t I_{batt} dt \tag{4.2.13}$$

Where SOC_0 is the initial State of Charge and Cap_{batt} is the total capacity of the battery. This equation accounts for the charge or discharge of the battery over time, allowing for an accurate calculation of the SOC, which is essential for managing the battery's performance and longevity. With the changes explained previously, the battery subsystem is shown in figure 4.23.

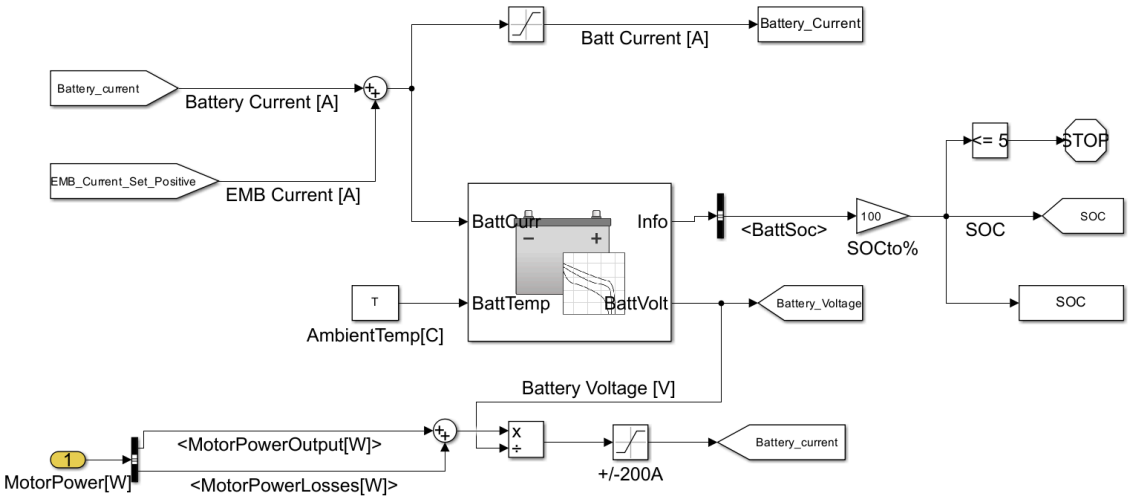

Figure 4.23: Improved Battery Subsystem

As shown in figure 4.23, the total current is calculated from the total power required by the motor by dividing it by the battery voltage:

$$I_{in} = \frac{P_{mtot}}{V_{out}} = \frac{P_m + P_{loss}}{V_{out}} \tag{4.2.14}$$

Additionally, the consumption due to the activation of the EMB when braking is included.

Changes on brake subsystem

As previously mentioned, the ECU of the brake-by-wire system must estimate the necessary braking force following the braking command and its intensity. Based on this estimation, it must efficiently distribute the braking force between friction braking and regenerative braking.

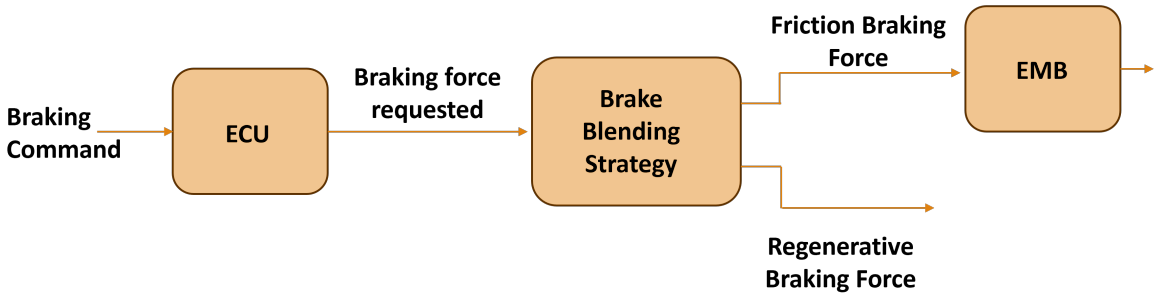

Figure 4.24: Brakes Scheme

An appropriate brake-by-wire model must necessarily account for these aspects. For this purpose, to estimate the necessary braking force, a relationship based on empirical data, specifically obtained for urban cycles, was used, linking the Brake Pedal Position (BPP), representing the braking command, to the deceleration rate.

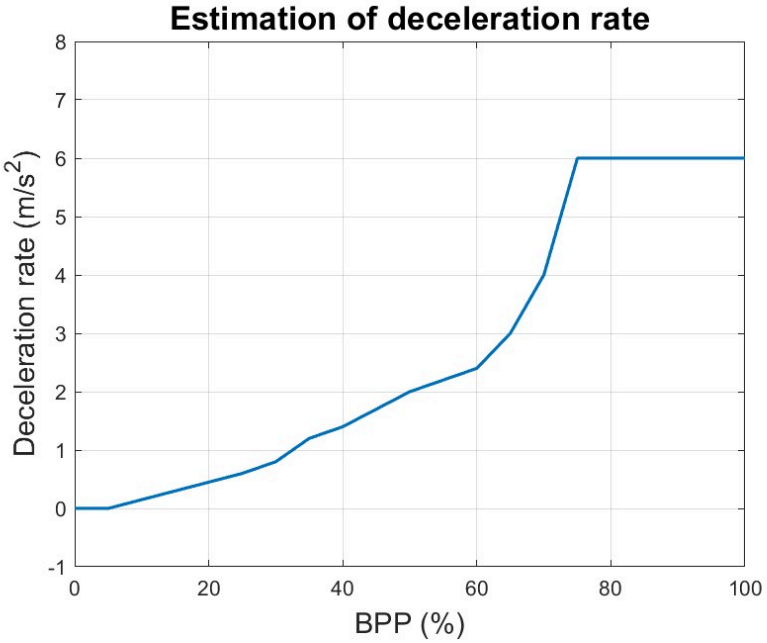

Figure 4.25: Estimation of deceleration rate

Once the deceleration rate is obtained, as shown in figure 4.25, the necessary

braking force is determined according to the following relation:

$$F_{brake} = \frac{a_{dec} m_{veh}}{\eta_{brake}} \tag{4.2.15}$$

where m_{veh} is the mass of the vehicle and η_{brake} is the brake efficiency. By introducing a rule based controller capable of understanding the intensity and type of braking request, this force is then divided into friction braking force and regenerative braking force. The brake blending stategy used, considers the braking intensity , $z = \frac{a}{g}$, where a is the actual deceleration of the vehicle, the maximum regenerative braking force of the system and the required braking force:

- $0 \leq z \leq 0.2$ When both the braking demand and intensity are low, the electric motor can entirely manage the braking, allowing for regenerative braking.
- $0.2 \leq < \leq 0.6$ In the case of moderate intensity, a combination of regenerative braking and friction braking is necessary to safely stop the vehicle. Specifically, the surplus braking demand that cannot be met through regenerative braking is handled by the friction brakes.
- $z > 0.6$ In emergency braking situations, represented by high braking intensity values, ensuring vehicle safety requires that the braking be managed exclusively by the friction braking system, excluding regenerative braking.

The maximum value of regenerative braking force directly depends on the electric motor used. The usual range of maximum braking torque obtainable through the electric motor varies between 10-50% of the maximum deliverable torque.In this case, a value of 30% T_{max} was used, reported on the wheel axis and converted into force by dividing by the wheel radius. Following this distribution, the friction braking portion is managed by the EMB model. It is important to note that the braking force produced by the EMB model is considered as the sum of the braking forces exerted on each wheel, thus assuming an equal distribution on each of them. As constructed, the model requires translating the braking force demand into a set clamping force. Considering a disc brake, the braking torque generated by the EMB can be expressed as:

$$T_{f\_EMB} = N_{pads} \mu_0 F_{cl} R_b \tag{4.2.16}$$

where N_{pads} is the number of brake pads, μ_0 is the coefficient of friction between the brake pads and the disk and R_b is the effective radius of the brake disc. Rearranging this equation and considering that $T_{brake} = F_{brake} r_{wheel}$:

$$F_{cl} = \frac{F_{brake} r_{wheel}}{N_{pads} \mu_0 R_b} \tag{4.2.17}$$

allowing to determine the required clamping force based on the braking request. Applying what has been explained, the diagram of the implemented brake subsystem is shown in the figure 4.26

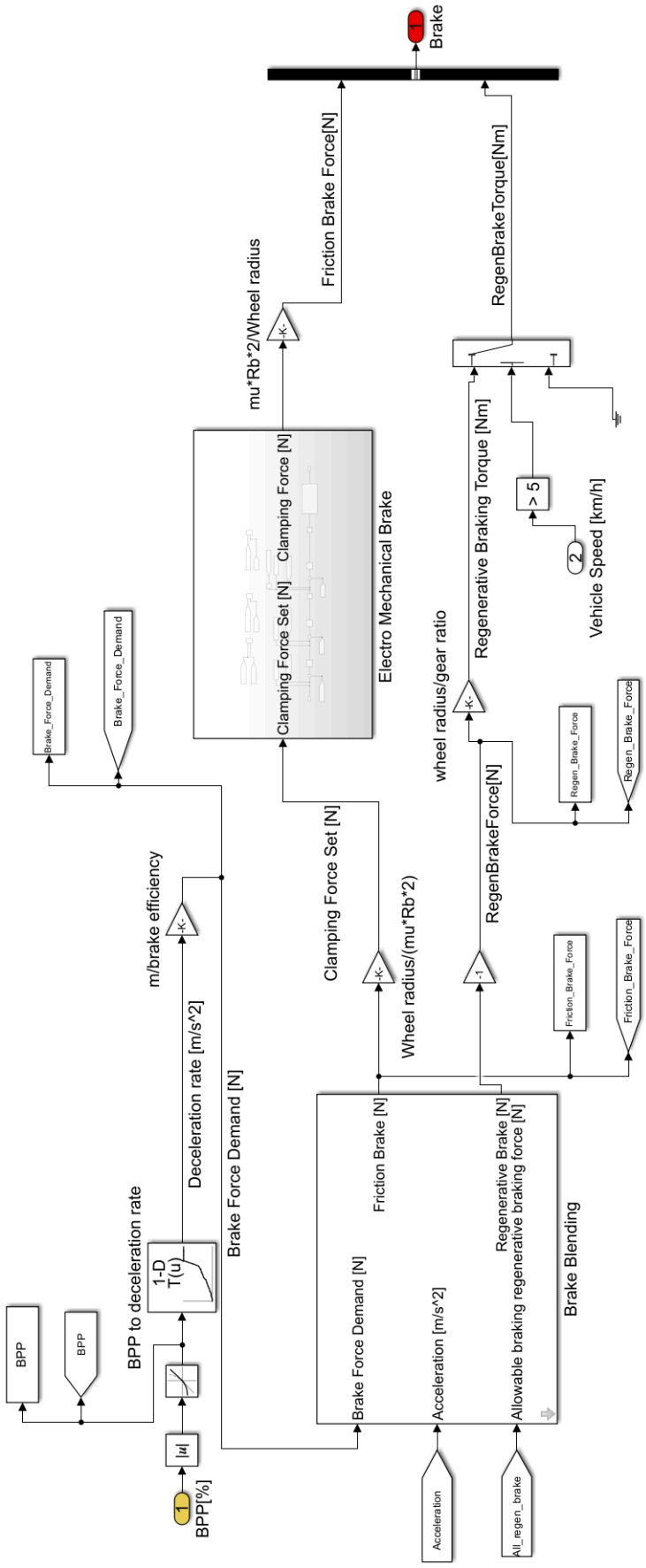

Figure 4.26: Improved Brake Subsystem

4.2.3 Parameters summary

In the following table, a summary of the parameters used to model the vehicle is provided:

Table 4.3: Vehicle Parameters Summary

m	vehicle mass	850 kg
r_w	wheel radius	0.2 m
A	vehicle frontal area	2.1 mˆ2
C_{rr}	rolling resistance coefficient	0.01
C_d	aerodynamic coefficient	0.3
θ	road angle	0 rad
ρ_{air}	air density	1.23 kg/mˆ3
T_{max}	Motor maximum torque	250 Nm
P_{max}	Motor maximum power	50 kW
T_{batt}	Battery temperature	300 K
S	Driveline spin loss	6 Nm
k	Allowable regenerative torque coefficient	0.3
G	Driveline trasnmission ratio	3.55
η_{br}	Brake efficiency	0.7
R_b	Brake disk radius	0.105 m

Chapter 5

Simulations and Results

For a comprehensive system analysis, it was initially necessary to focus on the stand-alone electromechanical brake model. After ensuring its consistent behavior and meeting the required specifications, simulations on the BEV model were subsequently carried out.

5.1 Simulations on EMB Model stand-alone

To analyze the behavior of the developed model and ensure that the system responds adequately to possible braking demands, simulations were conducted using step inputs of varying intensity for the clamping force set:

- Step Input of 5kN
- Step Input of 10kN
- Step Input of 15kN
- Step Input of 20kN

The use of a step input on the set clamping force allows for the analysis of the model's behavior in the worst-case scenario where the braking force demand is impulsive. These step inputs simulate different braking scenarios, from light braking to hard braking, allowing to observe how well the PID controllers manage the clamping force, motor speed, and motor current under varying conditions. This helps in verifying

that the system can handle different braking intensities effectively and maintain desired performance characteristics.

5.1.1 Step Input 5kN

The following graphs show the system response when a step input of 5kN on the set clamping force is requested.

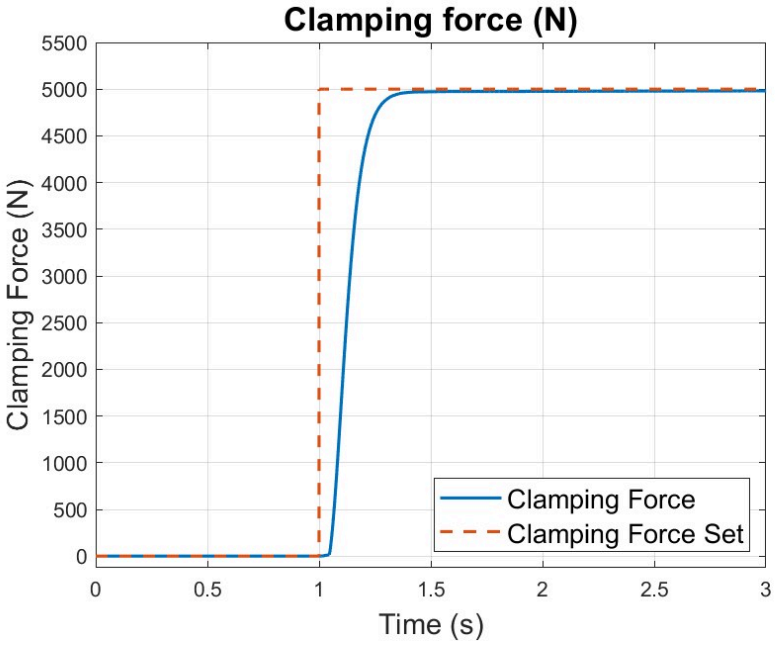

Figure 5.1: Clamping force

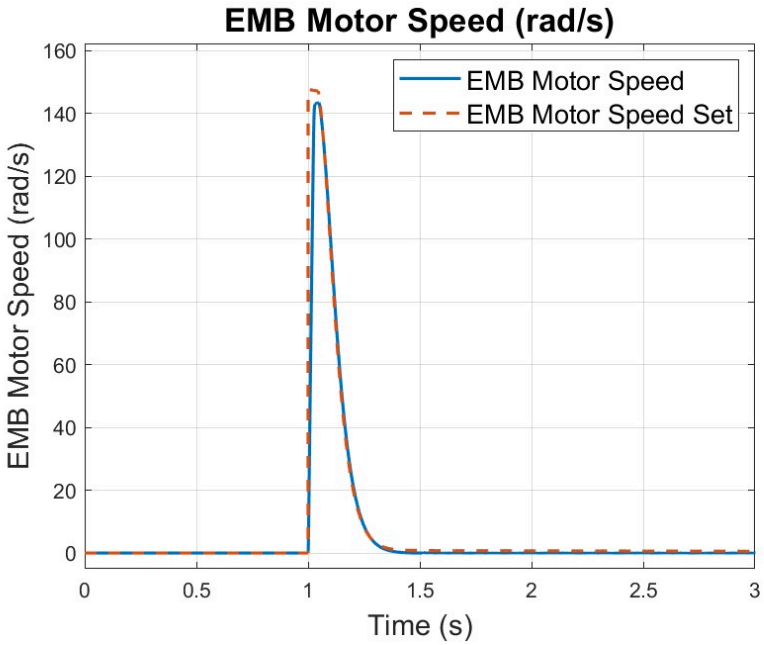

Figure 5.2: Motor speed

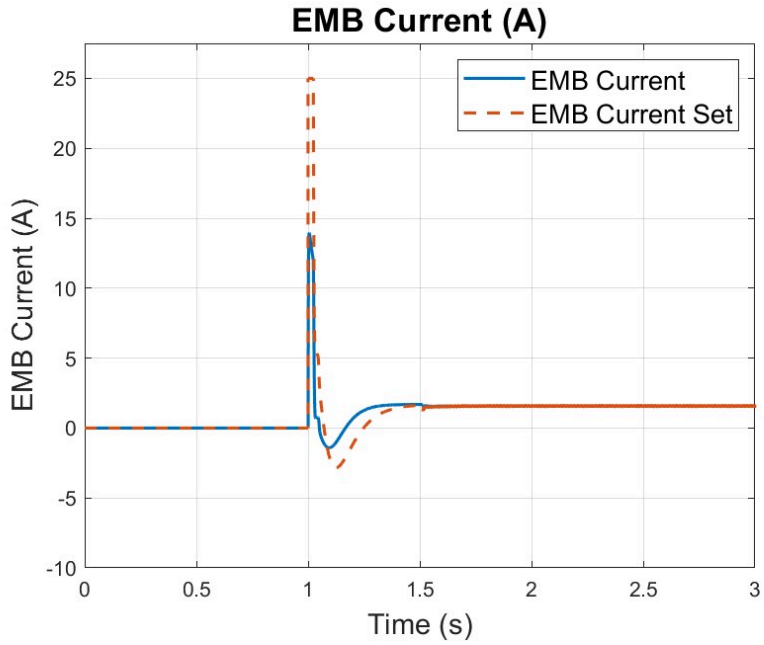

Figure 5.3: Current

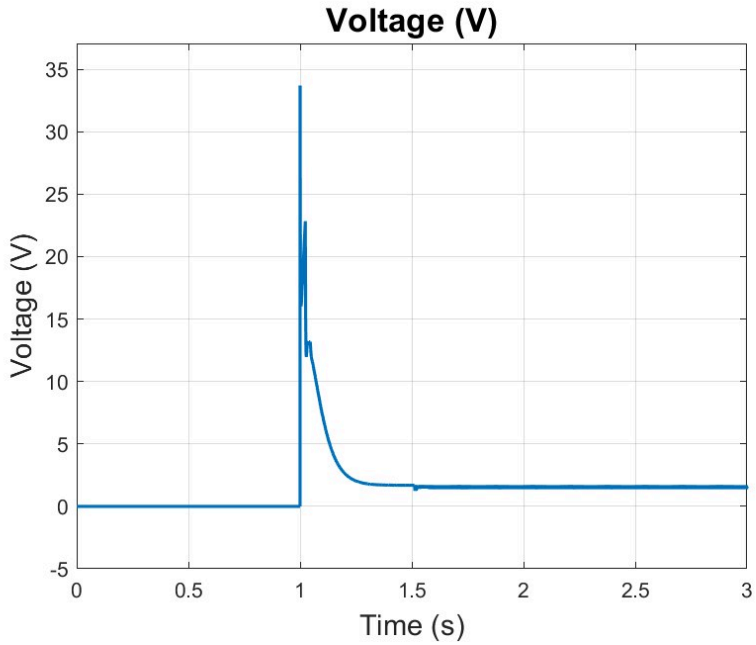

Figure 5.4: Voltage

Specifically, Figure 5.1 shows the clamping force obtained from the model as a solid line and the step setpoint as a dashed line. Figure 5.2 presents the actual rotational speed of the electric motor as a solid line and the motor speed setpoint, output from the outer control layer, as a dashed line. Figure 5.3 illustrates the actual current applied to the motor in a solid line, while the set current from the intermediate control layer is shown as a dashed line. Finally, Figure 5.4 displays the voltage applied to the motor armature terminals, obtained from the innermost control layer. This voltage is used to regulate the electric motor, thus becoming the input to the plant model. Following the application of the voltage, the electric motor activates after a brief moment. The motor's rotation is then translated into a linear displacement, which is associated with the generation of clamping force, as described in paragraph 4.1.

5.1.2 Step Input 10kN

The following graphs show the system response when a step input of 10kN on the clamping force is requested.

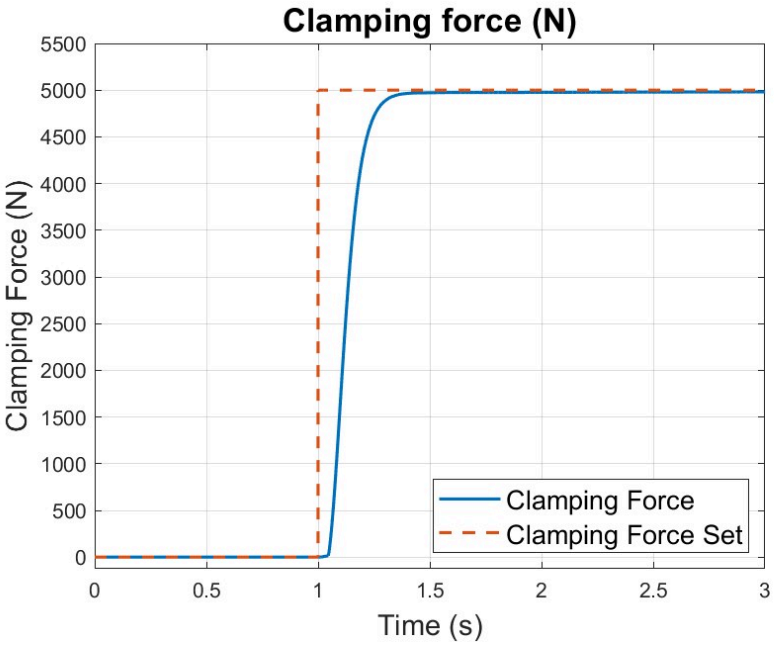

Figure 5.5: Clamping force

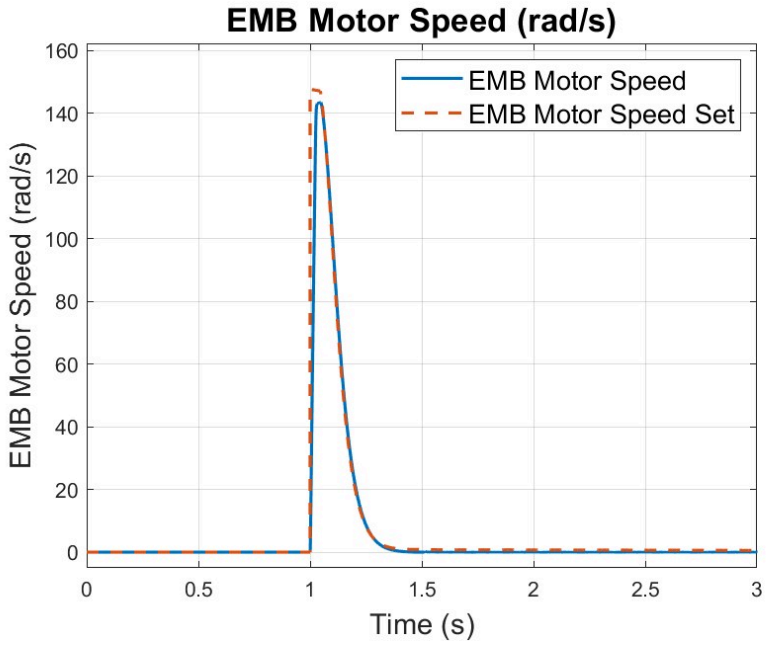

Figure 5.6: Motor speed

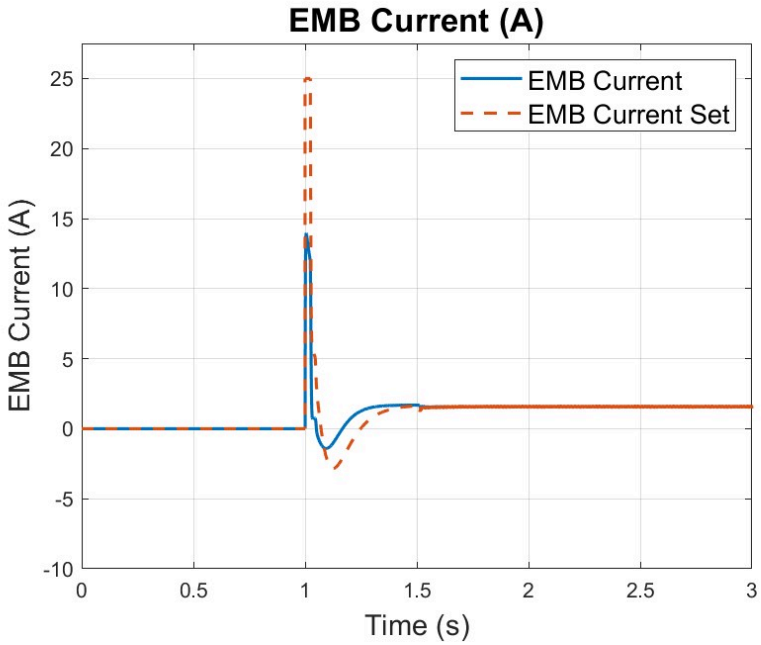

Figure 5.7: Current

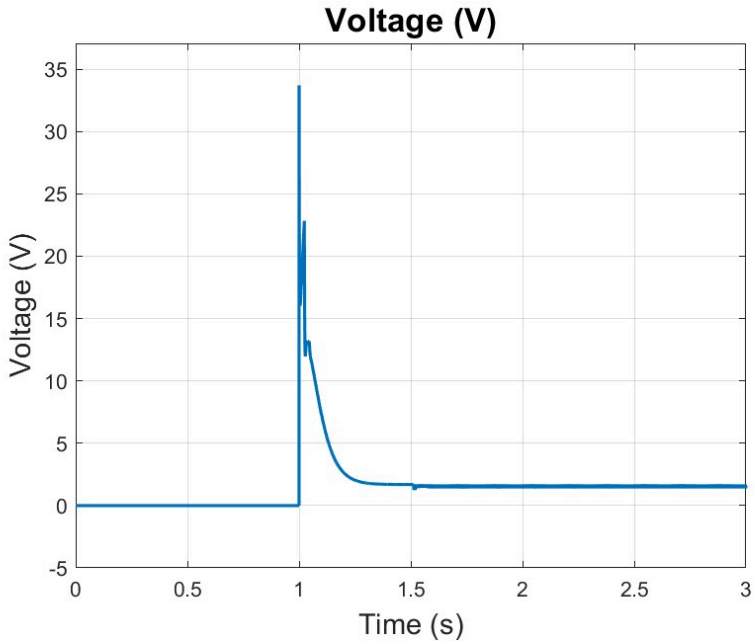

Figure 5.8: Voltage

Specifically, figure 5.5, shows the Clamping force Set and the clamping force obtained from the model, 5.6 shows the rotational speed of the electric motor, 5.7 shows the current applied to the motor, and 5.8 shows the voltage applied across the motor armature.

5.1.3 Step Input 15kN

The following graphs show the system response when a step input of 15kN on the clamping force is requested.

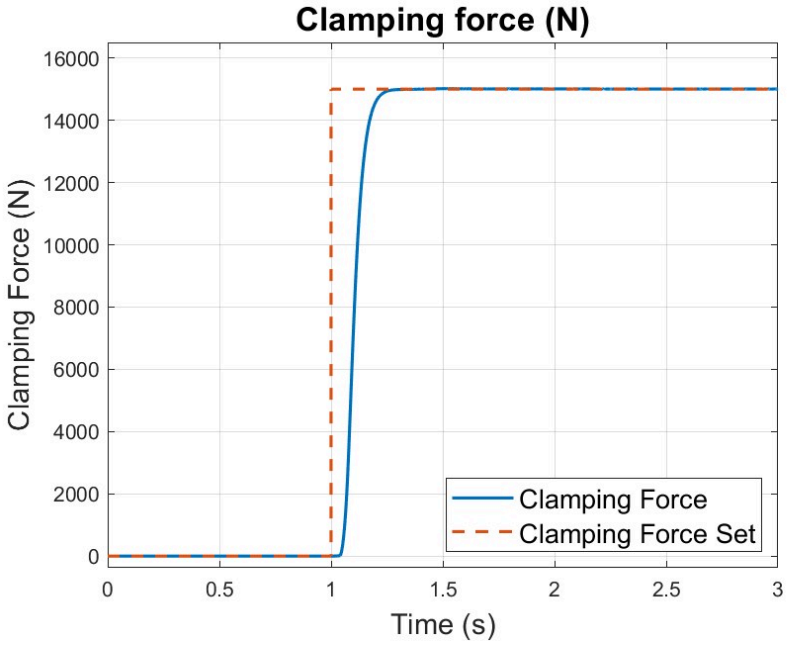

Figure 5.9: Clamping force

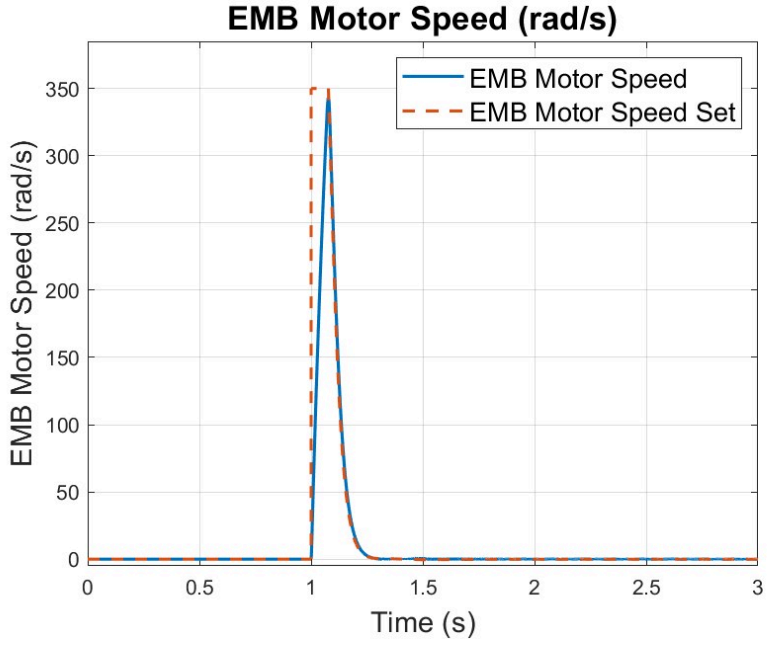

Figure 5.10: Motor speed

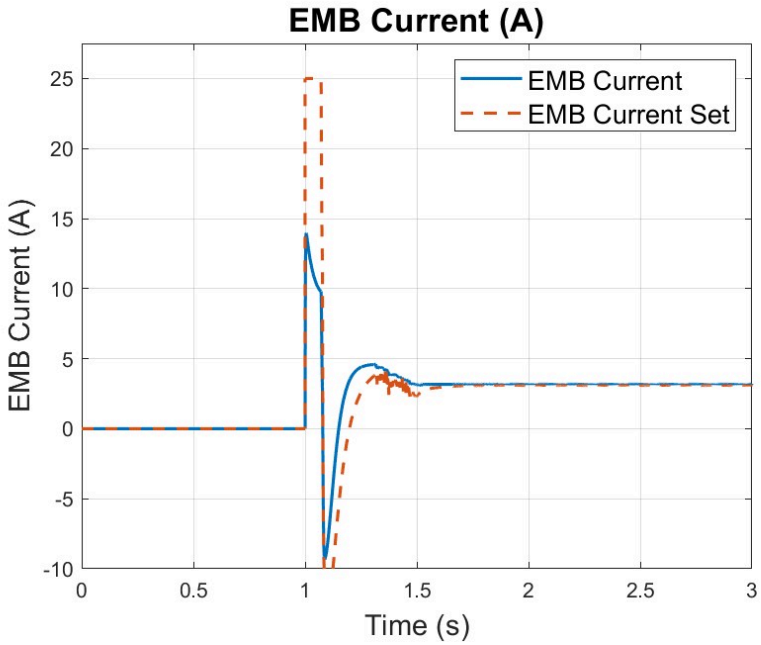

Figure 5.11: Current

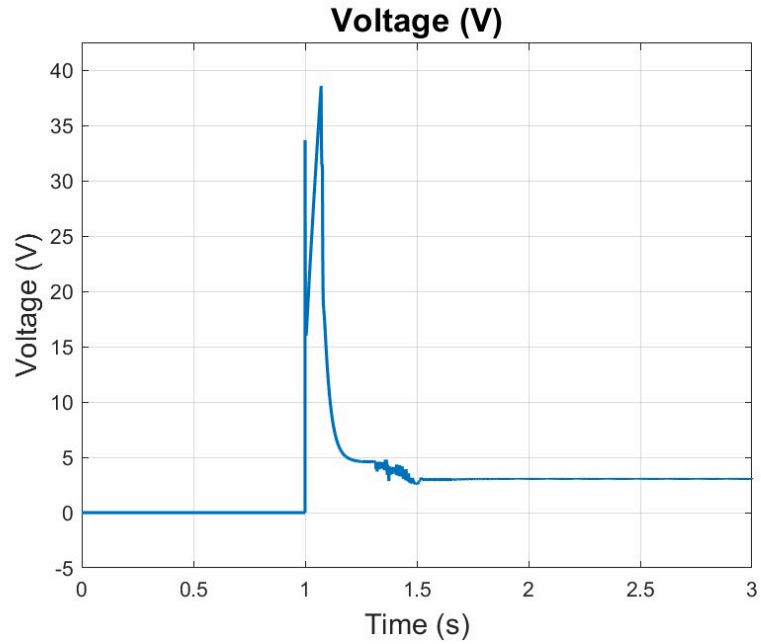

Figure 5.12: Voltage

Specifically, figure 5.9, shows the Clamping force Set and the clamping force obtained from the model, 5.10 shows the rotational speed of the electric motor, 5.11 shows the current applied to the motor and 5.12 shows the voltage applied across the motor armature.

5.1.4 Step Input 20kN

The following graphs show the system response when a step input of 20kN on the clamping force is requested.

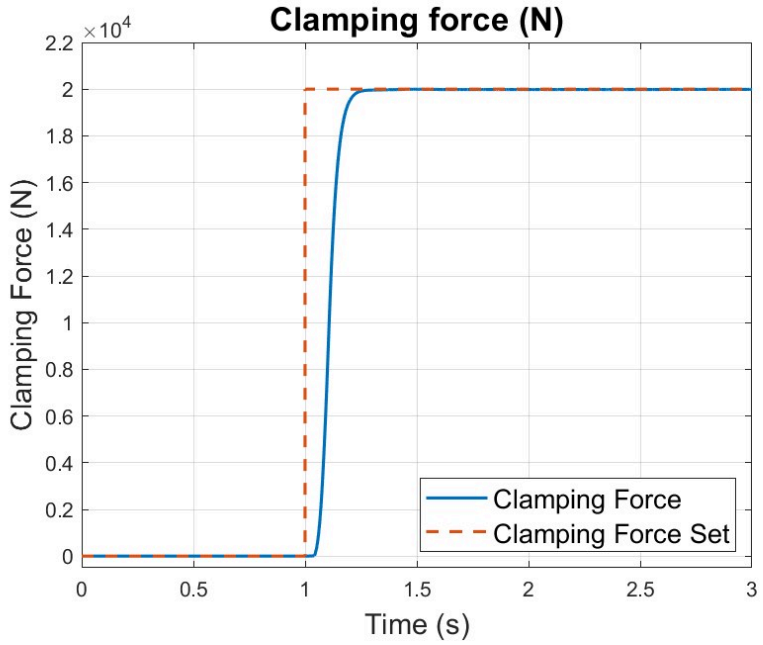

Figure 5.13: Clamping force

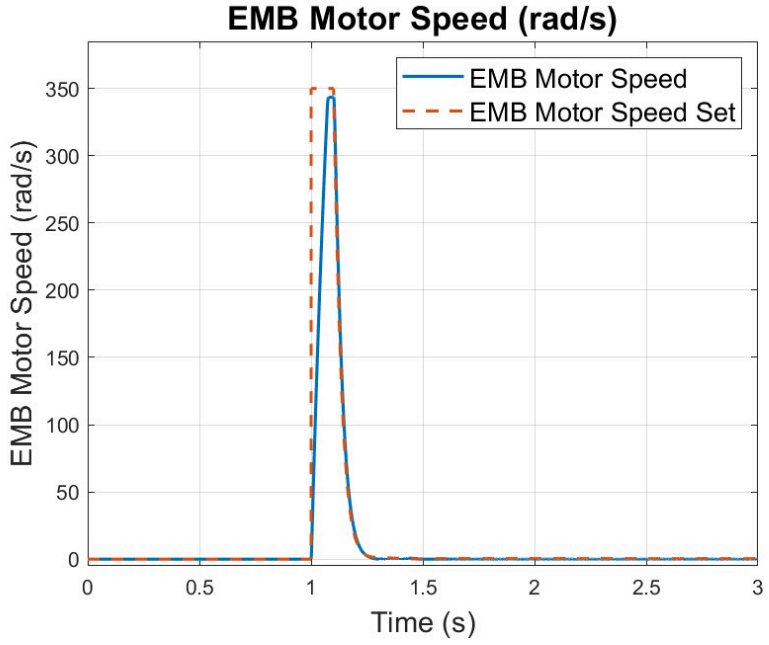

Figure 5.14: Motor speed

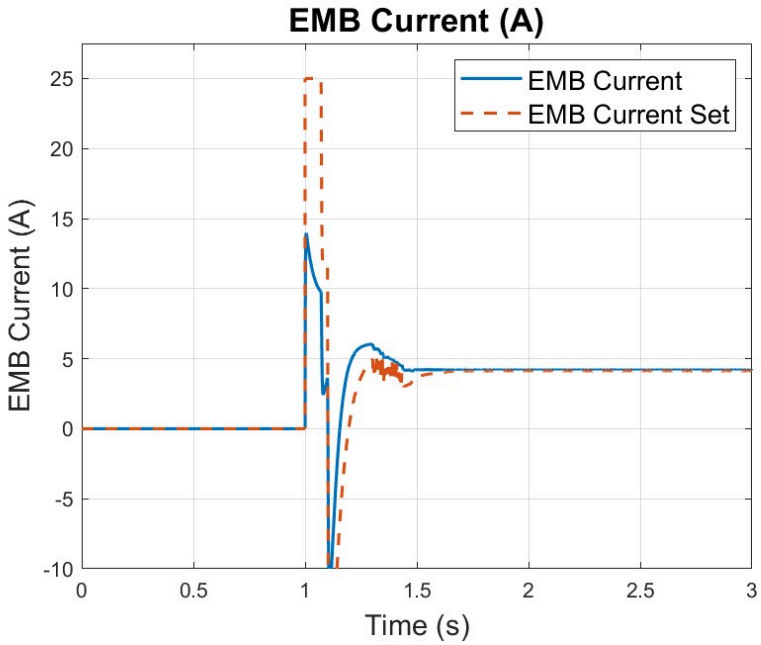

Figure 5.15: Current

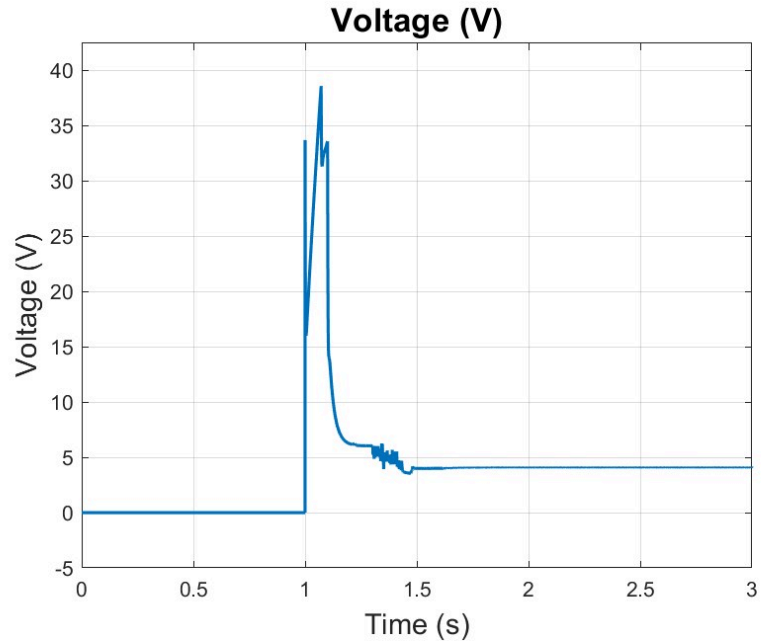

Figure 5.16: Voltage

Specifically, figure 5.13, shows the Clamping force Set and the clamping force obtained from the model, 5.14 shows the rotational speed of the electric motor, 5.15 shows the current applied to the motor and 5.16 shows the voltage applied across the motor armature.

5.1.5 Discussions

As can be seen from the figures 5.1,5.5,5.9 and 5.13, the system successfully follows the desired setpoint of clamping force in a satisfactory manner, adhering to the imposed mechanical and electrical limitations. For the first two cases, in the graphs 5.2 and 5.6 with an input of 5kN and 10kN, it can be observed that the motor rotation speed never reaches the maximum value of 350 rad/s, while in the remaining two 5.10 and 5.14, it is necessary to reach this value for a brief moment to achieve the desired clamping force. This suggests that for higher braking demands, an electric motor with better dynamic performance might be necessary. Despite this, considering the application of this system to small electric vehicles, the selected motor parameters are sufficient. Additionally, focusing on the current in the graphs 5.3, 5.7, 5.11 and 5.15, negative values can be observed. These are due to the need to decelerate the system once the required clamping force value is reached, which is related to the required motor rotation speed. To determine the system's response time, settling time, and error, it was necessary to define percentage value bands. Specifically:

- The response time is calculated as the time required to reach 100±2% of the maximum set clamping force.
- The settling time is defined as the time required for the response to remain within a 100±1% band of the maximum set clamping force.
- The error is the difference between the clamping force set and the average value of the clamping force obtained after the defined settling of the response.

This is graphically illustrated in the example figure 5.17.

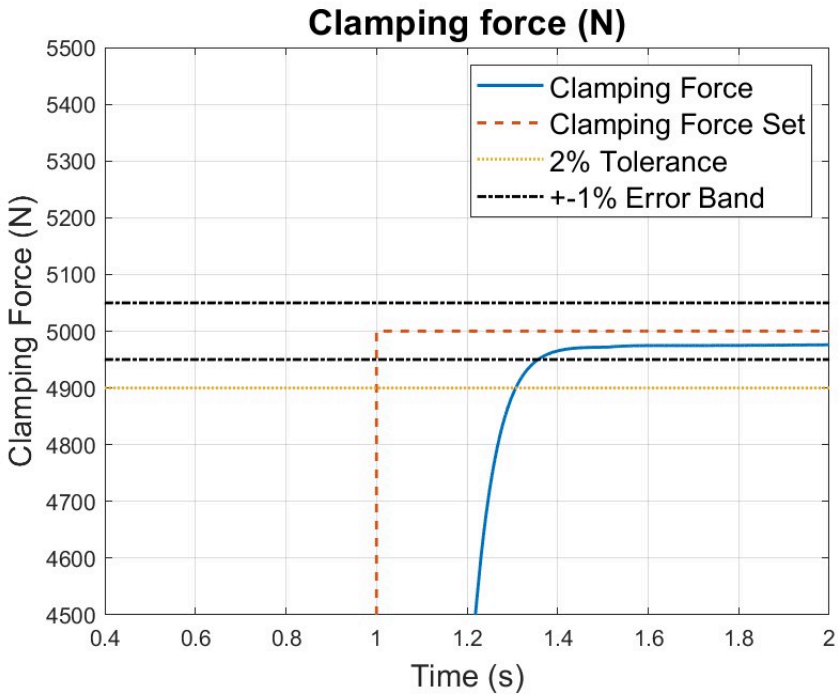

Figure 5.17: Clamping force and percentage bands

The following table summarizes the values obtained for each simulation.

Table 5.1: EMB Step Input Results

	5kN	10kN	15kN	20kN
Rising Time [s]	0.31	0.23	0.21	0.20
Settling Time [s]	0.36	0.26	0.23	0.22
Error [N]	18.04	-3.68	-5.06	10.94

The differences in response times and settling times, as well as the steady-state error, are due to the tuning of the PID parameters, which were optimized for input values of 20kN. This choice is motivated by the need for a better response to more intense braking demands, represented by higher values. Despite the small variations, the system exhibits response times in a range between 0.20 and 0.35 seconds, thereby meeting the required specifications for braking system response times of ECE R13 [36].

5.2 Simulations on BEV Model

The next step was to perform simulations on the BEV model presented in paragraph 4.2. To appropriately analyze the model's behavior, the following speed cycles were used:

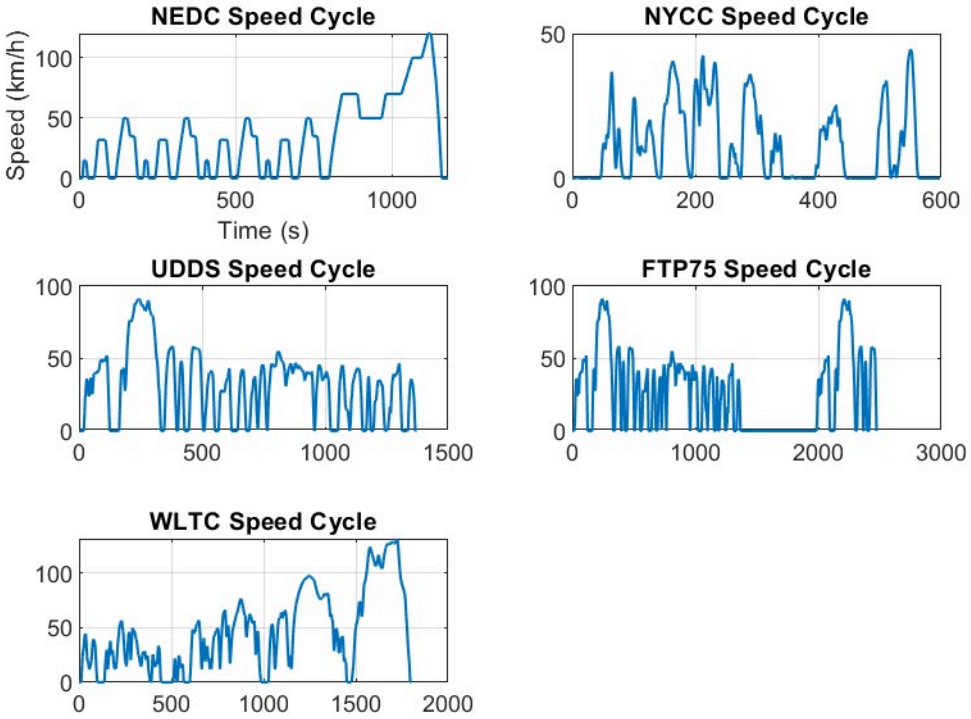

Figure 5.18: Speed Cycles

- NEDC (New European Driving Cycle): It consists of four urban cycles and one extra-urban cycle. The length of the cycle is 11.02 km, the duration is 1180 seconds, and the average speed is 33.63 km/h.
- NYCC (New York City Cycle): It simulates an urban cycle for light vehicles with frequent stops. The length of the cycle is 1.89 km, the duration is 598 seconds, and the average speed is 11.43 km/h.
- UDDS (Urban Dynamometer Driving Schedule): Also known as FTP72, it simulates an urban driving cycle composed of two phases. The length of the cycle is 12.07 km, the duration is 1369 seconds, and the average speed is 31.3

km/h.

- FTP75 (Federal Test Procedure): It adds a third phase to the UDDS following a long vehicle stop. The length is 17.78 km, the duration is 2474 seconds, and the average speed is 25.87 km/h.
- WLTC class3a (Worldwide harmonized Light vehicles Test Cycles): It consists of four phases: low, medium, high, and super high speed. The length of the cycle is 23.19 km, the duration is 1800 seconds, and the average speed is 46.39 km/h.

For brevity, the following paragraphs present only the results obtained using the UDDS and NYCC cycles.

5.2.1 Simulation with UDDS cycle

The results obtained using the UDDS (FTP-72) speed cycle are shown below.

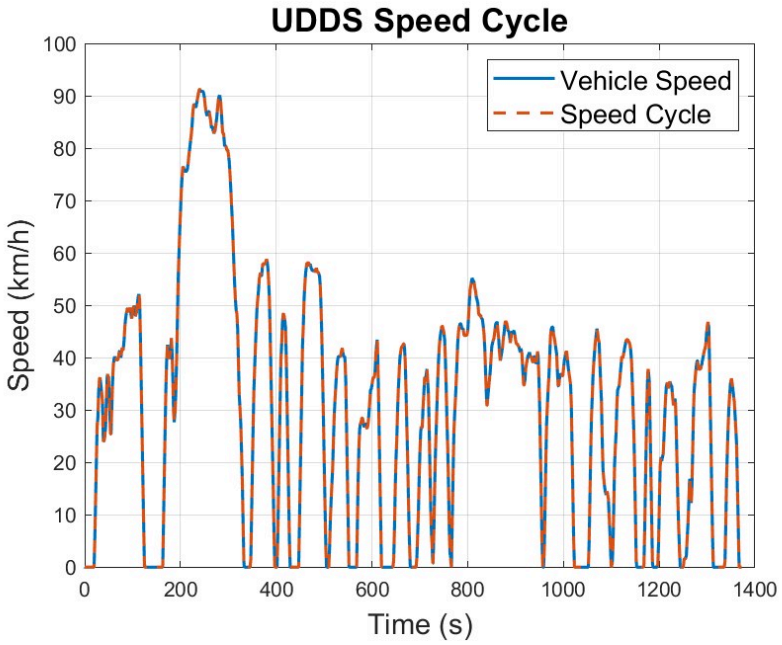

Figure 5.19: UDDS Vehicle Speed

In Figure 5.19, the actual vehicle speed derived from the model is shown with a solid line, while the reference speed of the UDDS cycle is shown with a dashed

line. As can be observed, the two speeds overlap except for a small error, which is depicted in Figure 5.20 with an added maximum error band of ±2 km/h.

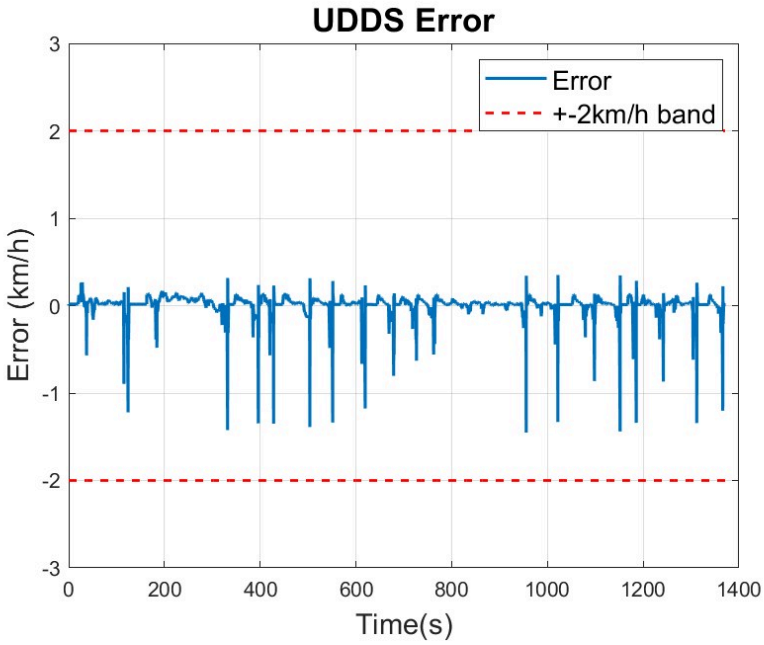

Figure 5.20: UDDS Speed Error

In Figure 5.21, the trend of the requested braking force is shown, divided into the braking force obtained through regeneration (shown in blue) and the braking force obtained through the EMB system (shown in red), as indicated in paragraph 4.2.2. Additionally, Figure 5.22 depicts the state of charge (SOC) of the vehicle's battery.

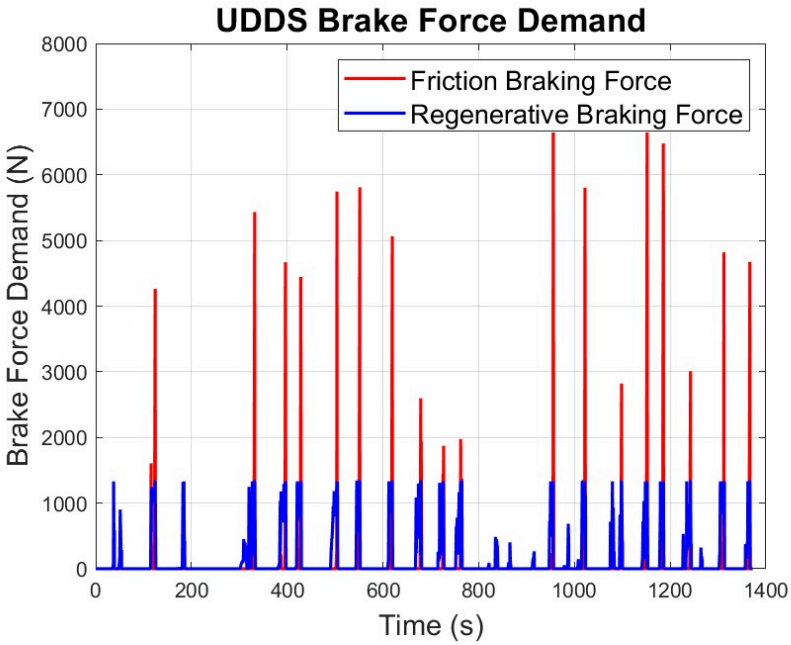

Figure 5.21: UDDS Brake Force Demand

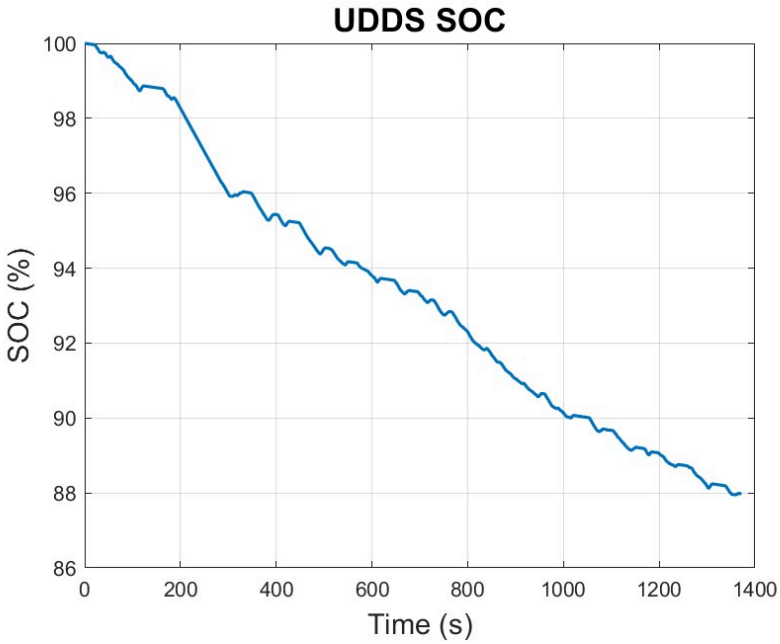

Figure 5.22: UDDS SOC

Referring to figures 5.20 and 5.21, the points where the error is larger correspond to the vehicle stops. At these moments, there are peaks in the required braking force. This behavior is mainly due to the use of the PID controller in the driver subsystem, which tends to reduce the error as quickly as possible, thereby requiring a higher

brake pedal position (BPP) and consequently a peak in the braking force necessary to stop the vehicle.

To verify the consistent behavior of the model, the results obtained by isolating one of the braking phases present in the cycle are also presented.

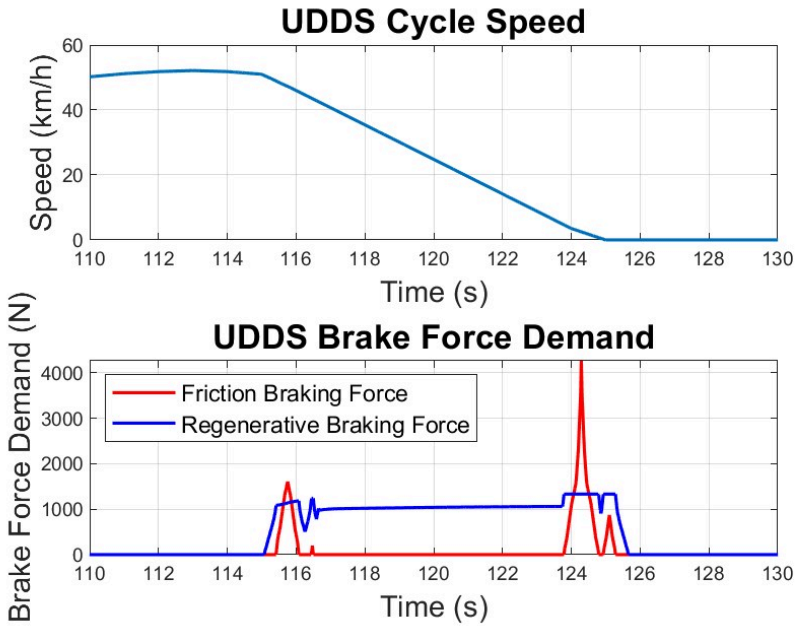

Figure 5.23: UDDS Zoom on vehicle speed and brake force demand

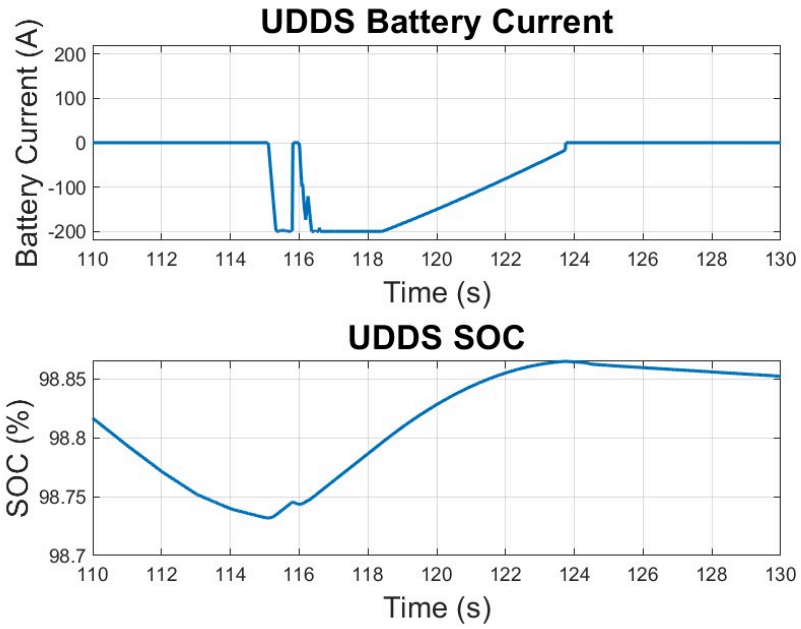

Figure 5.24: UDDS Zoom on current and SOC

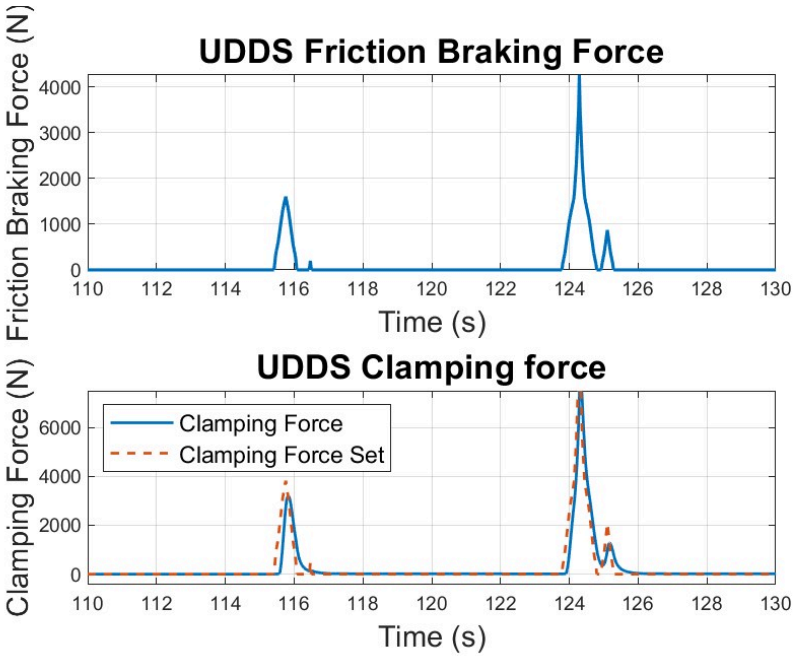

Figure 5.25: UDDS Zoom on friction braking force and clamping force

As can be seen from Figures 5.23 and 5.24, during the represented braking phase, the required braking force is partially distributed between regenerative braking and braking obtained through EMB. During instances of regenerative braking, the current assumes negative values, indicative of battery charging, which results in an increase in the SOC. The rise in current value around t=116s is due to the power consumption of the EMB, which becomes active at that moment. Furthermore, as explained in paragraph 4.2.2, the friction braking force required translates into a set clamping force for the EMB whose trend is shown in Figure 5.25.

5.2.2 Simulation with NYCC cycle

The results obtained using the NYCC speed cycle are shown below.

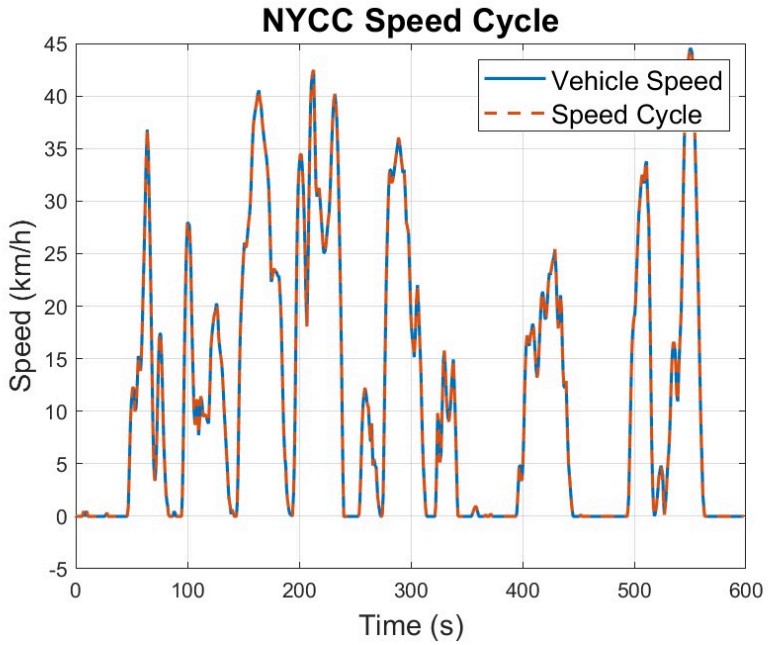

Figure 5.26: NYCC Vehicle Speed

In Figure 5.26, the actual vehicle speed derived from the model is shown with a solid line, while the reference speed of the NYCC cycle is shown with a dashed line. As can be observed, the two speeds overlap except for a small error, which is depicted in Figure 5.27 with an added maximum error band of ±2 km/h.

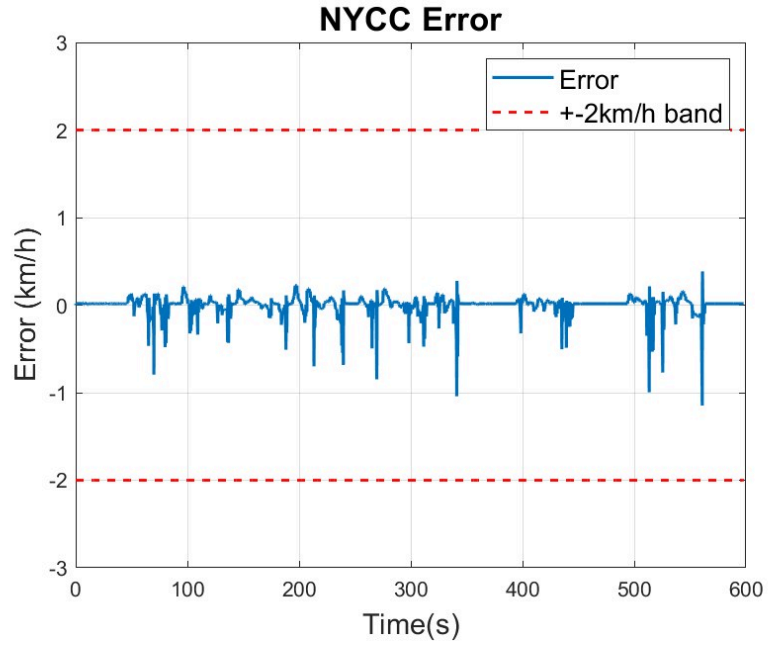

Figure 5.27: NYCC Speed Error

In Figure 5.28, the trend of the requested braking force is shown, divided into the braking force obtained through regeneration (shown in blue) and the braking force obtained through the EMB system (shown in red), as indicated in paragraph 4.2.2. Additionally, Figure 5.29 depicts the state of charge (SOC) of the vehicle's battery.

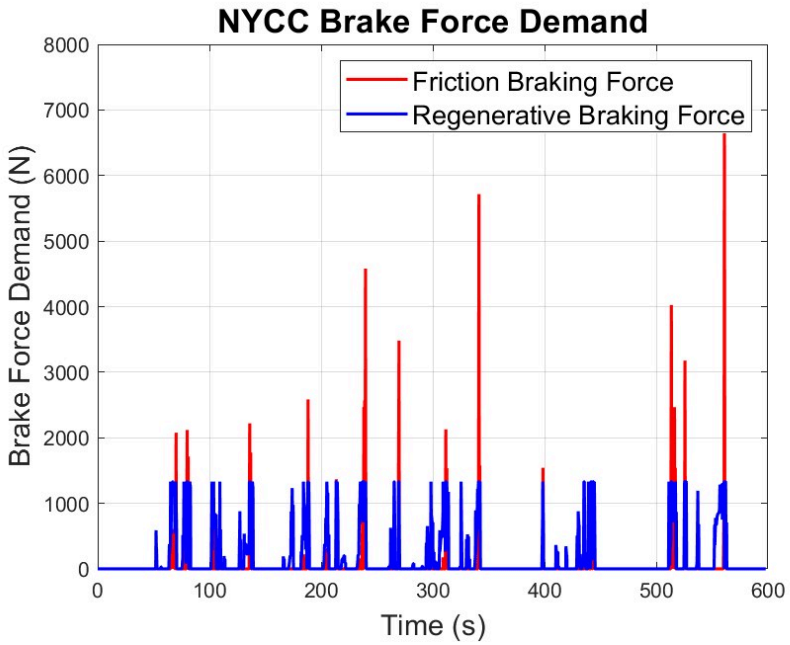

Figure 5.28: NYCC Brake Force Demand

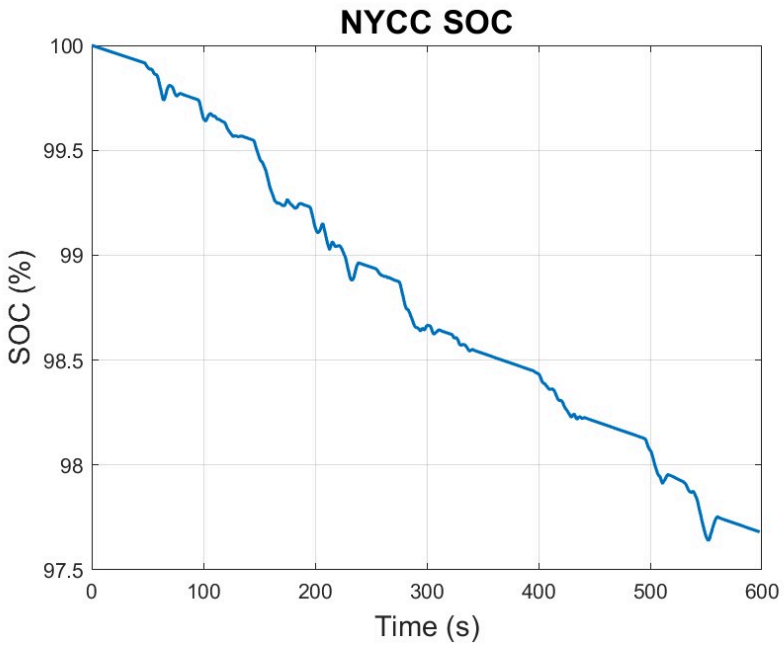

Figure 5.29: NYCC SOC

To verify the consistent behavior of the model, the results obtained by isolating one of the braking phases present in the cycle are also presented.

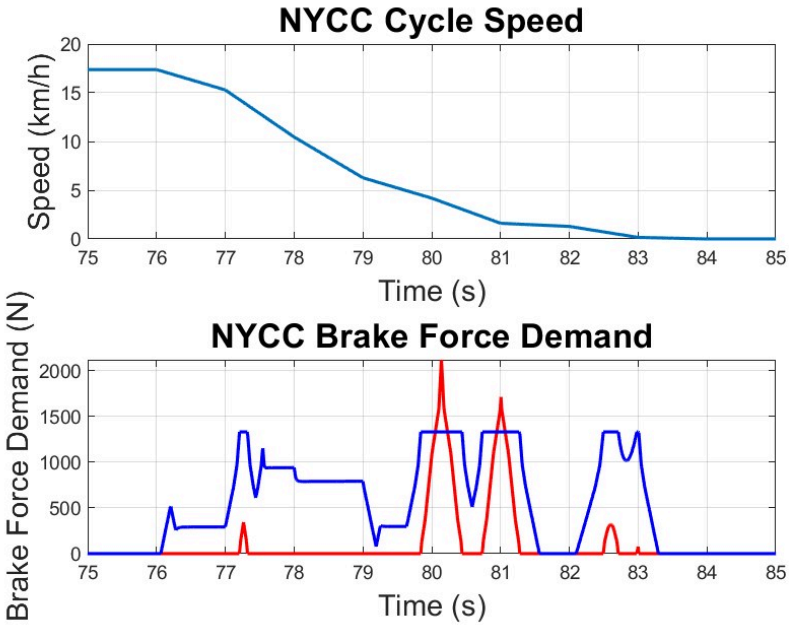

Figure 5.30: NYCC Zoom on vehicle speed and brake force demand

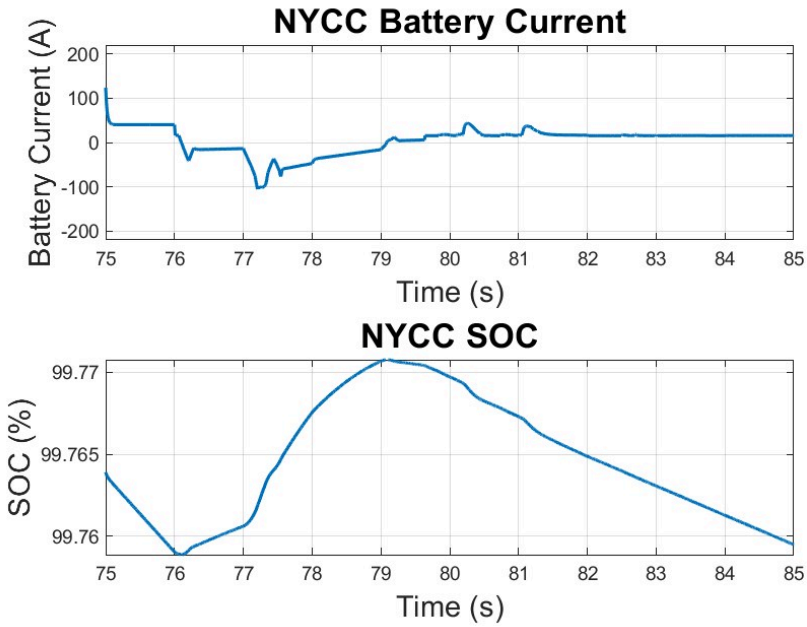

Figure 5.31: NYCC Zoom on current and SOC

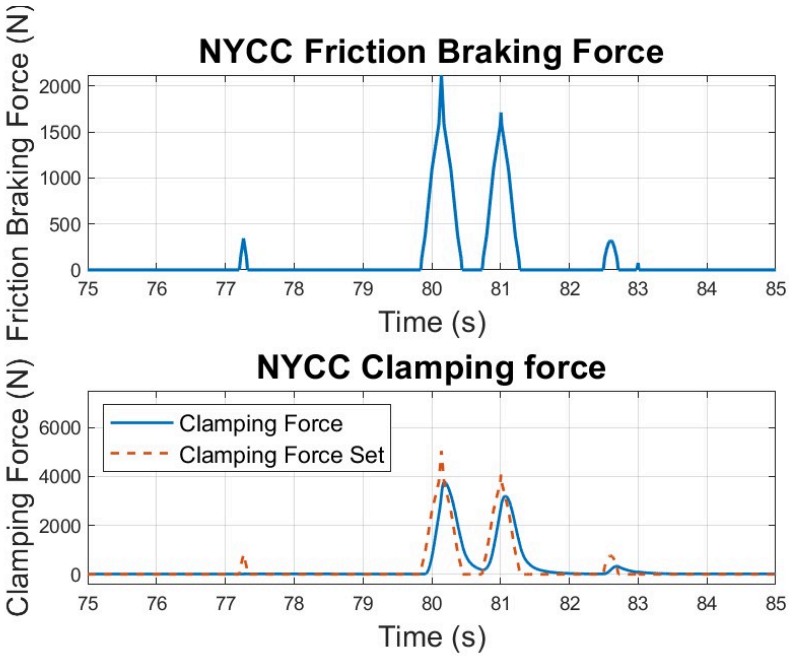

Figure 5.32: NYCC Zoom on friction braking force and clamping force

As can be seen from Figures 5.30 and 5.31, during the represented braking phase, the required braking force is partially distributed between regenerative braking and braking obtained through EMB. During instances of regenerative braking, the current assumes negative values, indicative of battery charging, which results in an increase in the SOC. Around t=80s, the contribution of braking force from the EMB is required, resulting in a consumption of the battery's SOC. Furthermore, as explained in paragraph 4.2.2, the friction braking force required translates into a set clamping force for the EMB whose trend is shown in Figure 5.32.

5.2.3 Simulation with UDDS cycle without regenerative braking

For completeness, the behavior of the model was also analyzed in the absence of regenerative braking with UDDS cycle. The results obtained are presented below.

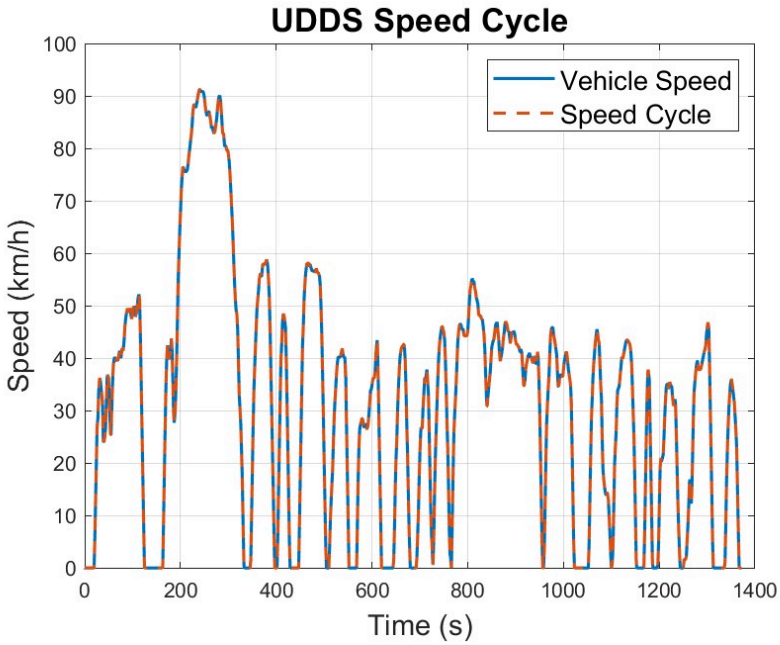

Figure 5.33: UDDS Vehicle Speed

In Figure 5.33, the actual vehicle speed derived from the model is shown with a solid line, while the reference speed of the UDDS cycle is shown with a dashed line. As can be observed, the two speeds overlap except for a small error, which is depicted in Figure 5.34 with an added maximum error band of ±2 km/h.

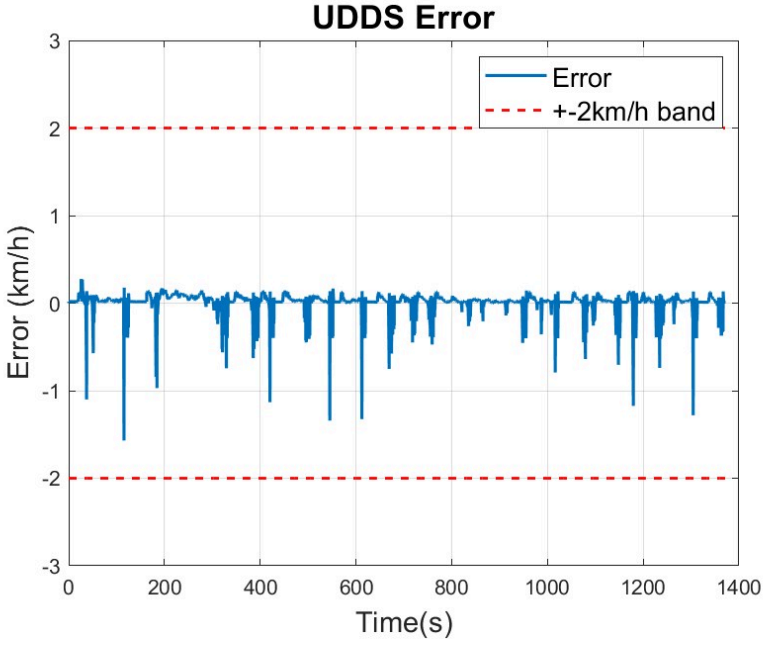

Figure 5.34: UDDS Speed Error

In Figure 5.35, the trend of the requested braking force is shown. In this case, with the regenerative component excluded, the braking demand is entirely managed by the EMB. Additionally, Figure 5.36 depicts the state of charge (SOC) of the vehicle's battery which is exclusively decreasing.

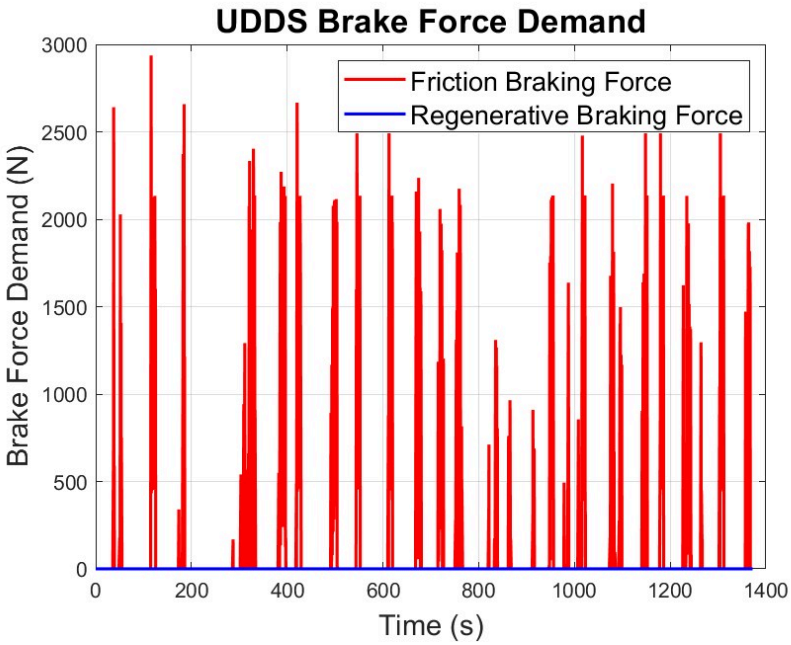

Figure 5.35: UDDS Brake Force Demand

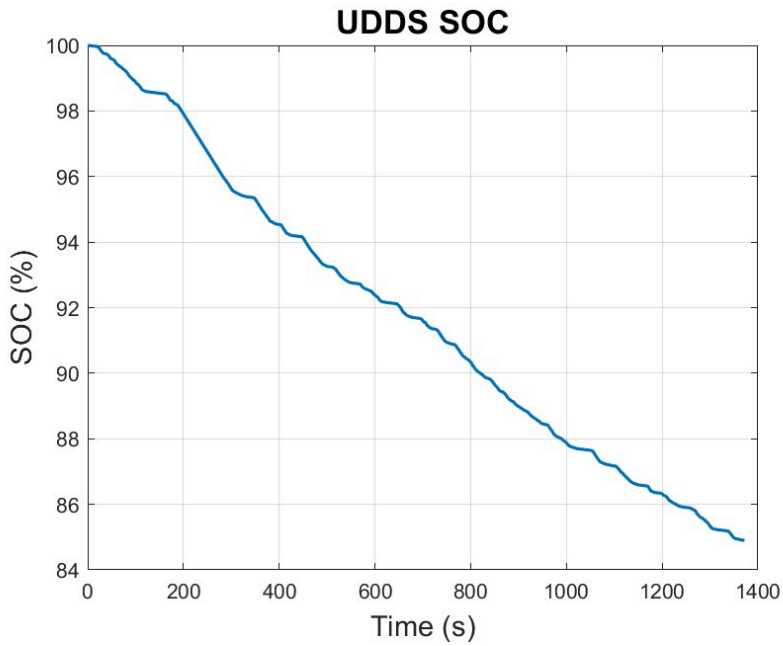

Figure 5.36: UDDS SOC

Referring to figures 5.34 and 5.35, the points where the error is larger correspond to the vehicle stops. At these moments, there are peaks in the required braking force. This behavior is mainly due to the use of the PID controller in the driver subsystem, which tends to reduce the error as quickly as possible, thereby requiring a higher brake pedal position (BPP) and consequently a peak in the braking force necessary to stop the vehicle.

To verify the consistent behavior of the model, the results obtained by isolating one of the braking phases present in the cycle are also presented.

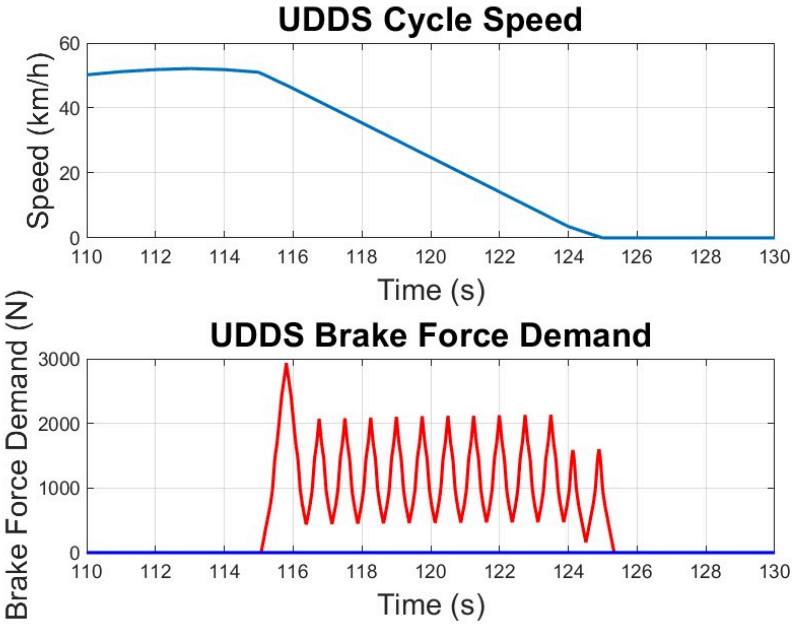

Figure 5.37: UDDS Zoom on vehicle speed and brake force demand

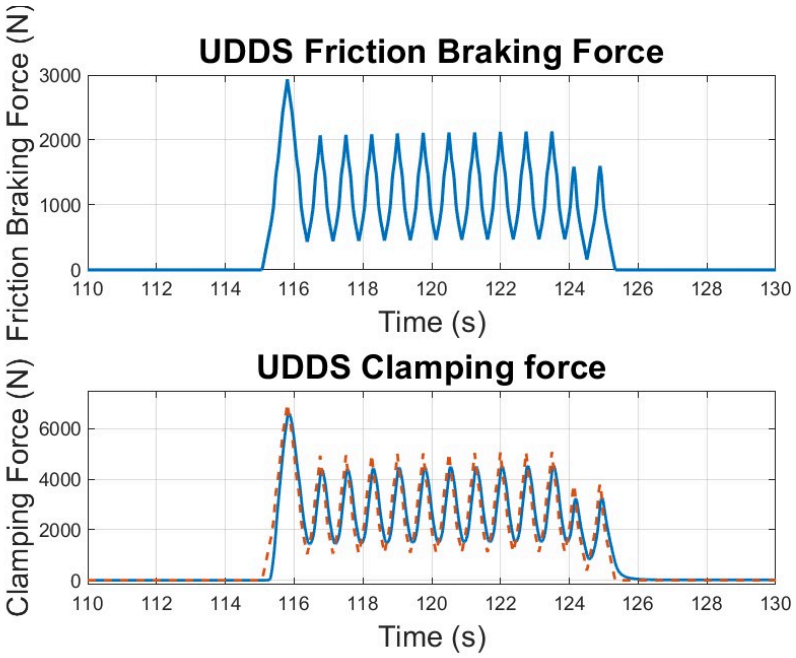

Figure 5.38: UDDS Zoom on friction braking force and clamping force

5.2.4 Discussions

As shown in Figures 5.19, 5.26 and 5.33, the vehicle speed satisfactorily follows the set speed, and the error between them falls within the ±2 km/h band for each cycle used. As can be seen from Figures 5.21 and 5.28, the cycles used are mainly characterized by light or moderate braking (paragraph 4.2.2, allowing for frequent use of regenerative braking. During instances where the contribution of the EMB is necessary, the developed model adequately responds to the braking demand, as highlighted in Figures 5.25 and 5.32. Furthermore, in cases where regenerative braking is excluded, as shown in Figures 5.35, 5.37 and 5.38, the developed EMB model adequately manages the braking force demand, ensuring that the speed error remains within the ±2 km/h band, shown in figure 5.34.
Finally, to evaluate the efficiency of the brake blending strategy, the state of charge of the battery is shown in figure 5.39, indicating the SOC trend with a blue line for the presence of regenerative braking and a red line for its absence.

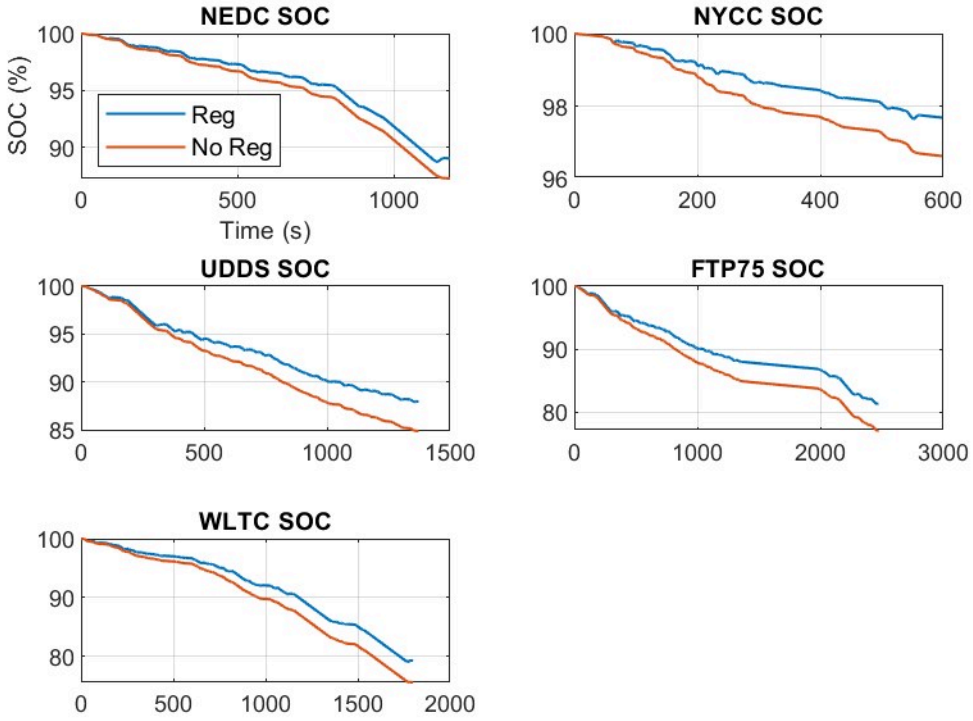

Figure 5.39: SOC variations

Using the data shown in Figure 5.39, it was possible to calculate the energy saving efficiency.

$$\eta_{rig} = \frac{\Delta SOC_{nr} - \Delta SOC_r}{\Delta SOC_{nr}} \tag{5.2.1}$$

where $\Delta SOC_{nr} = SOC_{in} - SOC_{fin\_nr}$ without regeneration and $\Delta SOC_r = SOC_{in} - SOC_{fin\_r}$ with regeneration. The following table summarizes the results obtained for each cycle.

Table 5.2: Speed Cycles Result Summary

	$SOC_{in}[\%]$	$SOC_{fin\_nr}[\%]$	$\Delta SOC_{nr}[\%]$	$SOC_{fin\_r}[\%]$	$\Delta SOC_r[\%]$	$\eta_{rig}[\%]$
NEDC	100	87.24	12.76	89.01	10.99	13.8
NYCC	100	96.62	3.38	97.68	2.32	31.36
UDDS	100	84.88	15.12	87.97	12.03	20.4
FTP75	100	78.33	21.67	82.27	17.73	18.18
WLTC	100	75.54	24.46	79.25	20.75	15.8

It is important to note that the SOC percentage value shown in the table 5.2 represents the percentage of the battery's usable range. The regenerative braking efficiency of electric vehicles has significantly improved, and the efficiency ofregenerative braking reaches more than 13%. The highest efficiency values are obtained using the NYCC cycle, where the average speed is the lowest.

Chapter 6

Conclusions

In conclusion, in this thesis work, a digital twin of an EMB applied to a battery electric vehicle was developed. Analyzing the results obtained, the developed EMB model can be used to test different brake control logics in order to achieve better dynamic performance. Following the modeling of the EMB, a simple rule-based braking distribution strategy was defined for implementation within the BEV model, resulting in a battery SOC saving. The developed model can be used to improve braking management strategies, to connect it to an external system such as the Traffic Management System (TMS) and for appropriate component sizing. Considering the results obtained, further future study is necessary for the distribution of braking force on each wheel to ensure vehicle stability and prevent wheel lockup.

Bibliography

[1] Alexandros Nikitas, Kalliopi Michalakopoulou,Eric Tchouamou Njoya and Dimitris Karampatzakis, 2020, Artificial Intelligence, Transport and the Smart City: Definitions and Dimensions of a New Mobility Era https://doi.org/10.3390/su12072789

[2] Gkartzonikas, C., Gkritza, K. (2019). What have we learned? A review of stated preference and choice studies on autonomous vehicles. Transportation Research Part C: Emerging Technologies, 98, 323-337.

[3] Cohen, T., Cavoli, C. (2019). Automated vehicles: Exploring possible consequences of government (non)intervention for congestion and accessibility. Transport Policy, 66, 1-9.

[4] Betina Carol Zanchin; Rodrigo Adamshuk; Max Mauro Santos; Kathya Silvia Collazos, 2017, On the Instrumentation and Classification ofAutonomous Cars, 10.1109/SMC.2017.8123022

[5] Dixit, U. S., Kant, R., Ravi Kumar, M., Muralidharan, N. (2016). Brake-by-Wire System: An Overview. IEEE Transactions on Vehicular Technology, 65(8), 5797-5806.

[6] https://www.teoresigroup.com/it/about/

[7] Simscape Multibody - MATLAB & Simulink - MathWorks Website, https://it.mathworks.com/products/simmechanics.html

[8] Bauer, W., Becker, M., Gerlach, T. (2018). Brake-by-Wire—Safety Concept, Mechanisms and Vehicle Dynamics Control Functionality. SAE Technical Paper Series.

[9] Xuehui HuaJinbin ZengHaoxin Li, 2023, A Review of Automobile Brake-by-Wire Control Technology

[10] Hsieh, S. S., Lin, C. S., Chou, J. C. (2019). Development of an Electro-Hydraulic Brake-by-Wire System for Electric Vehicles. IEEE Access, 7, 156832-156840.

[11] Perricone, G., Da Lio, M., Savaresi, S. M., Velardocchia, M. (2020). Advanced Brake-by-Wire Systems for Electrified Vehicles: A Comprehensive Review. IEEE Transactions on Vehicular Technology, 69(5), 4516-4534.

[12] El Baghdadi, M., Bossche, P. V. D., Hegazy, O., Omar, N. (2018). An Advanced Electric Brake Pedal for Electric Vehicles: Development and Performance Evaluation. Energies, 11(10), 2718.

[13] D'alfio, N.; Morgando, A.; Sorniotti, A. Electro-hydraulic brake systems: Design and test throughhardware-in-the-loop simulation. Veh. Syst. Dyn. 2006, 44, 378–392.

[14] Yong, J.; Gao, F.; Ding, N.; He, Y. Design and validation of an electro-hydraulic brake system using hardware-in-the-loop real-time simulation. Int. J. Automot. Technol. 2017, 18, 603–612.

[15] Xiaoxiang Gong, Weiguo Ge, Juan Yan, 2020, Review on the Development, Control Method and Application Prospect of Brake-by-Wire Actuator

[16] Li, J.; Ding, M.; Yong, W.; Li, C. Evaluation and Optimization of the Nonlinear Flow Controllability ofSwitch Valve in Vehicle Electro-Hydraulic Brake System. IEEE Access 2018, 6, 31281–31293.

[17] Zhi-Hui Tan, Zhen-Fu Chen, Xiaofei Pei, 2016, Development of integrated electro-hydraulic braking system and its ABS application. 10.1007/s12541-016-0042-8

[18] Michael Flad, Simon Rothfuss, Gunter Diehm, Soeren Hohmann, 2024, Active Brake Pedal Feedback Simulator Based on Electric Drive. 10.4271/2014-01-0325

[19] ZF Friedrichshafen $press.zf.com/press/en/media/media_6$3488.$html$

[20] Chenhua Hu et al 2023, Research of Brake by Wire System. J. Phys.: Conf. Ser. 2479 012051

[21] Continental AG $https://www.continental-automotive.com/en/components/brake-systems.html$

[22] Congcong Li et al. 2023 Review of Electro-Mechanical Brake (EMB) System: Structure, Control and Application. https://doi.org/10.3390/su15054514

[23] Tuantuan Li et al. 2019 Research on Mechanism and Key Technology of Intelligent Vehicles Brake By Wire system. 10.1109/CVCI47823.2019.8951547

[24] Bosch GmbH, Automotive Brake Systems, 1996

[25] Bosch GmbH, Automotive Brake Systems, SAE International 1996

[26] Bosch GmbH, Safety, Comfort and Convenience Systems, 2006

[27] Maron, C.; Dieckmann, T.; Hauck, S.; Prinzler, H. Electromechanical Brake System: Actuator Control Development System; Technical Report, SAE Technical Paper; SAE: Vienna, Austria, 1997.

[28] Schwarz, R.; Isermann, R.; Böhm, J.; Nell, J.; Rieth, P. Modeling and Control of an Electromechanical Disk Brake; Technical Report, SAE Technical Paper; SAE: Vienna, Austria, 1998.

[29] Jo, C.; Hwang, S.; Kim, H. Clamping-force control for electromechanical brake. IEEE Trans. Veh. Technol. 2010, 59, 3205–3212.

[30] Line, C.; Manzie, C.; Good, M. Robust Control of an Automotive Electromechanical Brake. IFAC Proc. Vol. 2007, 40, 579–586.

[31] Krishnamurthy, P.; Lu, W.; Khorrami, F.; Keyhani, A. Robust Force Control of an SRM-based Electromechanical Brake and Experimental Results. IEEE Trans. Control. Syst. Technol. 2009, 17, 1306–1317.

[32] Saric, S.; Bab-Hadiashar, A.; Hoseinnezhad, R. Clamp-Force Estimation for a Brake-by-Wire System: A Sensor-Fusion Approach. IEEE Trans. Veh. Technol. 2008, 57, 778–786.

[33] www.tec-science.com/mechanical-power-transmission/planetary-gear

[34] Jian Li , Xingmin Xiao , Zhong kai Li , Chi Ma, 2023, Research on Electro-Mechanical Brake Systems Control Method for Mine Underground Electric Trackless Rubber-Tired Vehicle. doi:10.20944/preprints202308.1735.v1

[35] Pennestrì, E., Rossi, V., Salvini, P. et al. Review and comparison of dry friction force models. Nonlinear Dyn 83, 1785–1801 (2016). https://doi.org/10.1007/s11071-015-2485-3

[36] United Nations Economic Commission for Europe. "ECE Regulation No. 13: Uniform Provisions Concerning the Approval of Vehicles of Categories M, N and O with Regard to Braking." https://unece.org/transport/vehicle-regulations-wp29/ece-regulations-motor-vehicles.

[37] 3CEMS Group, $https : //www.3cems.com/the - 6 - levels - of - vehicle - autonomy_n 69$

[38] W.A. Shanaka P. Abeysiriwardhana and A.M. Harsha S. Abeykoon, Simulation of Brake by Wire System with Dynamic Force Control

[39] Jing Li, Tong Wu,Tianxin Fan, 2020, Clamping force control of electro-mechanical brakes based on driver intentions. 10.1371/journal.pone.0239608